NEURAL EXTENDED KALMAN FILTER BASED ANGLE-ONLY TARGET TRACKING FOR CRUISE MISSILES

A THESIS SUBMITTED TO
THE GRADUATE SCHOOL OF NATURAL AND APPLIED SCIENCES
OF
MIDDLE EAST TECHNICAL UNIVERSITY

BY

GÖRKEM EŞSİZ

IN PARTIAL FULFILLMENT OF THE REQUIREMENTS
FOR
THE DEGREE OF MASTER OF SCIENCE
IN
AEROSPACE ENGINEERING

JANUARY 2016

Approval of the thesis

NEURAL EXTENDED KALMAN FILTER BASED ANGLE-ONLY TARGET TRACKING FOR CRUISE MISSILES

submitted by **GÖRKEM EŞSİZ** in partial fulfillment of the requirements for the degree of **Master of Science in Aerospace Engineering Department, Middle East Technical University** by,

Prof. Dr. Gülbin Dural Ünver _________________
Dean, Graduate School of **Natural and Applied Sciences**

Prof. Dr. Ozan Tekinalp _________________
Head of Department, **Aerospace Engineering**

Asst. Prof. Dr. Ali Türker Kutay _________________
Supervisor, **Aerospace Engineering Dept.,METU**

Examining Committee Members:

Prof. Dr. Ozan Tekinalp _________________
Aerospace Engineering Dept.,METU

Asst. Prof. Dr. Ali Türker Kutay _________________
Aerospace Engineering Dept.,METU

Prof. Dr. Kemal Leblebicioğlu _________________
Electrical and Electronics Engineering Dept.,METU

Asst. Prof. Dr. İlkay Yavrucuk _________________
Aerospace Engineering Dept.,METU

Asst. Prof Dr. Coşku Kasnakoğlu _________________
Electrical and Electronics Engineering Dept.,TOBB UET

Date: ________________

I hereby declare that all information in this document has been obtained and presented in accordance with academic rules and ethical conduct. I also declare that, as required by these rules and conduct, I have fully cited and referenced all material and results that are not original to this work.

Name, Last name : Görkem Eşsiz

Signature :

ABSTRACT

NEURAL EXTENDED KALMAN FILTER BASED ANGLE-ONLY TARGET TRACKING FOR CRUISE MISSILES

Eşsiz, Görkem
M.S., Department of Aerospace Engineering
Supervisor: Asst. Prof. Dr. Ali Türker Kutay

January 2016, 64 Pages

The main issue in the angle only target tracking problem is to estimate the states of a target by using noise corrupted measurement of elevation and azimuth. The states consist of relative position and velocity between the target and the platform. In this thesis the tracking platform is a sea skimming anti-ship missile (SS-ASM) with an active radar seeker. Normally, an active radar seeker gives the information of relative range and closing velocity to the target together with line of sight (LOS) angle and line of sight rate of elevation and azimuth. However, when a missile is jammed, the missile cannot give the information of relative range between itself and the target yet can measure LOS angles and LOS rates. In the jammed environment, to estimate the range from the LOS and LOS rate measurements, the missile has to maneuver to ensure the observability for range estimation.

Since sea skimming anti-ship missiles keep constant altitude during flight, which is almost below 10 or 5 meters, elevation channel is not included through the estimation and it is assumed that the missile moves only in horizontal plane. Another issue for SS-ASMs is target velocity and maneuverability profile. Missiles are much faster than ship targets. Thus stationary and constant velocity targets are examined through the thesis.

Two different approaches for range estimation are investigated and compared on simulated data: the standard Extended Kalman Filter (EKF) and the Neural Extended Kalman Filter (NEKF). The system model for estimation is formulated in terms of Modified Spherical Coordinates (MSC) for 2D horizontal missile-target geometry. Different platform maneuvers to obtain observability are studied and the geometry of the simulation scenario is investigated. Moreover, enhancement of the NEKF based estimation algorithm is introduced.

Keywords: Angle-only Target Tracking, Range Estimation, Neural Extended Kalman Filter, Modified Proportional Navigation Guidance Law

ÖZ

SEYİR FÜZELERİ İÇİN SİNİR AĞI GENİŞLETİLMİŞ KALMAN FİLTRE TABANLI ÖLÇÜM AÇILARINA BAĞLI HEDEF TAKİBİ

Eşsiz, Görkem
Yüksek Lisans, Havacılık ve Uzay Mühendisliği Bölümü
Tez Yöneticisi: Yrd. Doç. Dr. Ali Türker Kutay

Ocak 2016, 64 Sayfa

Ölçüm açılarına bağlı hedef takibindeki asıl sorun gürültültüyle bozulmuş yunuslama ve yalpalama açı ölçümlerini kullanarak hedef durumlarının kestiriminin yapılmasıdır. Bu hedef durumları, hedef ve füze arasındaki göreceli pozisyon ve hızı içermektedir. Bu tezde, takip eden gözlemci su sathından uçan ve gemilere karşı kullanılan aktif radar arayıcıya sahip bir füzedir. Normal koşullarda aktif radar arayıcı başlık kalan mesafe, yaklaşma hızı, Görüş Hattı (GH) açısı ve GH açısal hız ölçümlerini sağlamaktadır. Fakat, hedef savunma sistemleri tarafından parazit yayın yapan bir bozucu varken füze radar arayıcı başlığı kalan mesafe biligisini sağlayamaz ama GH açı ve GH açısal hız biliglerini ölçmeye devam eder. Bu durumda GH açısı ve GH açısal hız ölçümlerini kullanarak kalan mesafe kestiriminin yapılabilimesi ve kestirim sırasında gözlemlenebilirliğin devamlı olarak sağlanabilimesi için füze manevralar gerçekleştirmelidir.

Gemi hedeflerine karşı su sathından uçan füzeler sabit irtifadan ve yaklaşık 5-10 metreden uçtukları için kalan mesafe kestiriminde yunuslama kanalı dahil edilmemiş ve füzenin sadece yatay düzlemde manevra gerçekleştirdiği varsayılmıştır. Ayrıca füze hızı hedef gemiye göre daha büyük olduğu için bu tezde sabit hedef ve sabit hızlı hedef profilleri incelenmiştir.

Mesafe kestirimi için iki farklı yaklaşım üzerinde durulmuş ve koşulan benzetimler karşılaştırılmıştır: Genişletilmiş Kalman Filtresi ve Sinir Ağı Genişletilmiş Kalman filtresi. Sistem modeli 2 boyutlu yatay füze-hedef geometrisi için Modifiye Küresel Kordinatlarda ifade edilmiştir. Gözlemlenebilirliği sağlamak için farklı füze manevraları araştırılmıştır. Geliştirilmiş Sinir Ağı Genişletilmiş Kalman filtre tabanlı algoritma sunulmuştur.

Anahtar Kelimeler: Ölçüm Açılarına Bağlı Hedef Takibi, Kalan Mesafe Kestirimi, Sinir Ağı Genişletilmiş Kalman Filtresi, Modifiye Orantılı Seyir Güdüm Kanunu

ACKNOWLEDGEMENTS

First of all, I would like to express my sincere gratitude to my supervisor Asst. Prof. Dr. Ali Türker Kutay for his guidance and support throughout the thesis study.

I am very thankful to my colleagues and friends Gökcan Akalın and Suzan Kale Güvenç for sharing their invaluable experiences on the subject of my thesis.

I would like to extend my appreciation to my dear friends; Murat Akyol, Osman Çınar, Anday Demirsoy and Mehmet Emin Tuna for their endless support and friendship.

I owe my thanks to my parents Bahar Eşsiz and İdris Eşsiz for their endless love, encouragements and support for my whole life. I am also thankful to my aunt Arzu Öngel Öztürk, my aunt's husband Sinan Öztürk and my brilliant cousin Ata Öztürk.

Special thank and deepest gratitude to my dearest Naz Tuğçe Öveç for her endless encouragement and love. Without her support, this work would not have been completed.

TABLE OF CONTENTS

LIST OF FIGURES

FIGURES

LIST OF TABLE

TABLES

CHAPTER 1

INTRODUCTION

Introduction to the thesis work is given in this chapter. First background and literature survey in the area is presented. Thereafter scope of thesis and contributions are presented. Finally the thesis is outlined.

1.1 Background

Anti-ship missiles (ASM) are designed against ships and large boats. Most ASMs are all-weather and sea skimming missiles. Sea skimming is a feature that most anti-ship missiles use to be not detected by defense radar during their approach.

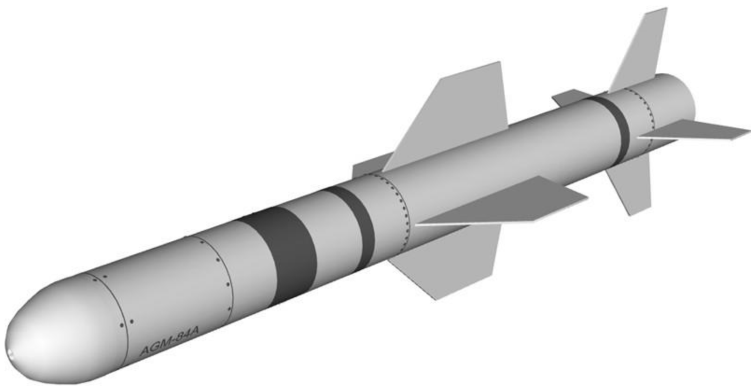

Figure 1.1-1 AGM-84A Harpoon 3D Model. The Harpoon is an all-weather, over the horizon, anti-ship missile system.

Sea skimming anti-ship missiles (SS-ASM) flies at 5-10 meters over the sea so that targets cannot detect sea skimming missiles until they come into view over the horizon. By flying few meters over the sea, detection range by the target ships is reduced significantly. However, sea skimming feature can increase the risk of water impact with the missile because of high waves in rogue weather conditions.

SS-ASMs are usually equipped with active radar seekers to detect other vehicles and targets. Active radar seekers give information of azimuth and elevation LOS, LOS rate and relative range between the missile and the target by measuring the time it takes for a radar pulse to travel from the transmitter to the target and back. However, when a SS-ASM equipped with active radar seeker becomes jammed, the seeker cannot measure the relative range between itself and the target but can measure LOS angles and LOS rates.

1.2 Literature Survey

Relative range information between a missile and a target can be used in terminal phase of the flight in order to increase the guidance performance of the missile [1]. Active radar seeker can give the range information but when it encounters with a jammer then it cannot sense relative range anymore. However, seeker still measures the LOS angles and LOS rates. With the measured angles and angle rates the range can be estimated if the missile maintains appropriate maneuvers to guarantee the observability.

The estimation of target position and velocity based on angle measurements is called angle-only target tracking, passive ranging or bearing-only-tracking. The problem of angle-only target tracking is well studied. The fundamental of target tracking that is given in Ref. [2]. Ref. [3] covers most aspects of tracking and has one chapter which explains only target tracking problem. Ref. [4] shows and compares different types of tracking methods.

Since the angle-only target tracking problem has nonlinear nature, nonlinear filtering techniques are required for the tracking solution. Due to the fact that Cartesian coordinates are simple to implement, it is used extensively for target tracking with extended Kalman filter (EKF). In Cartesian coordinates system model is linear and measurement model is highly nonlinear. However, it is revealed that the filter with Cartesian coordinates shows unstable behavior characteristics [5]. In Ref. [6], the system is formulated in Modified Spherical Coordinates (MSC) which is well suited for angle-only target tracking. This coordinate system decouples the observable and unobservable components of the state vector.

Observability is the other issue in target tracking problem. Observability requirements are investigated for only the constant velocity trajectory case in two [7] and three dimensions [8]. Detailed works on observability can be found also in Ref. [9, 10, 11, 12]. Implementation of pseudolinear filter for bearing-only target motion analysis can be found in Ref. [13] with observability analysis. In MSC, if there is no observer maneuver (no acceleration), reciprocal of range becomes unobservable even if the target is stationary or moving with constant velocity. However, in Ref [14] it is stated that as long as there is LOS rate in the system, the range can be estimated even there is no observer maneuver for stationary targets. Thus, for the stationary target cases, system equations given in Ref. [6] should be modified so that range could be estimated when the observer has no maneuver.

In this thesis, to obtain observability for the target tracking problem two different maneuver types are investigated. First one is the sinusoidal trajectory of the observer known as weaving maneuver. This maneuver is also used at terminal phase of the SS-ASM to escape target ships defense systems. Another maneuver is obtained by using modified proportional navigation guidance (MPNG) as guidance law at terminal phase of the observer. MPNG law is used for short-range air-to-air intercept scenarios for missiles which have IR seeker so far. Detailed studies can be found in Ref. [15, 16, 17].

Even if the full observability is obtained through the target state estimation problem, true states cannot be estimated exactly with standard EKF and there will remain gaps between the true states and the estimated states. At this point, Neural Extended Kalman Filter (NEKF) can be used to fill these gaps. NEKF is introduced first in Ref. [18]. Main idea of the NEKF is to reduce effects of unmodeled dynamics, mismodeling, extreme nonlinearities and linearization in the standard EKF [19]. Obtained improvement by using NEKF instead of EKF in the system model provides more accurate state estimate. Weights in the NEKF are coupled with EKF states and the weights are trained by Kalman gains [20].

There are several areas of usage of NEKF. For instance, errors in sensor measurements may emerge from different sources such as noise and sensor limitations which may result in biases. In these cases calibration for the sensor model can be achieved by NEKF [21, 22]. Another area of usage is the tracking problems with interacting multiple models (IMM). The NEKF algorithm is used to improve motion model prediction during the target maneuver [23, 24, 25, 26, 27]. Moreover, NEKF is used for the missile intercept time calculation [28, 29].

Extended Kalman filter, neural extended Kalman filter and required maneuver types to obtain observability in target tracking problem with modified spherical coordinates are studied in this thesis. The necessary analyses are conducted and obtained results are presented.

1.3 Scope of This Thesis

In this thesis, the angle-only target tracking problem for stationary and constant velocity target types is investigated. Modified spherical coordinates are used as the coordinate system. Two different estimation methods are studied during this thesis. The first method is the extended Kalman filter and the second one is the neural extended Kalman filter. General purpose of this thesis is to reveal advantages and disadvantages of neural extended Kalman filter based range estimation.

1.4 Contributions

The contributions of this work can be summarized as follows:

- Although the range estimation with angle-only measurements is referred in the literature, there is not documented real sea-skimming anti-ship missile application exists.
- Observability analysis of the estimation is described both numerically and theoretically.
- Sinusoidal movement of the observer to get observability is studied. Maneuver amplitude and period with obtained estimation results are given explicitly.
- The modified proportional navigation guidance law is the other method to obtain observability in this thesis. MPNG is investigated in detail and used for radar seeker equipped sea skimming anti-ship missiles.
- NEKF is implemented with Cartesian coordinates for the interacting multiple model tracking filters in the literature. In this thesis, NEKF is implemented and derived with modified spherical coordinates.

1.5 Outline of the thesis

In Chapter 2, the basis of angle-only target tracking is introduced and the coordinate systems are given. Thereafter observability issue and the necessary maneuver types to obtain observability are discussed. In Chapter 3, the theory of the EKF and NEKF is presented. In Chapter 4, from LOS angle and LOS rate measurements provided by RF seeker, the range estimation is performed both with the EKF and the NEKF. Also, an estimation comparison with sinusoidal motion and MPNG is studied and the results of these analyses are presented. In Chapter 5, conclusions of this work are given.

CHAPTER 2

ANGLE ONLY TARGET TRACKING

In angle-only target tracking main idea is to estimate the target position and the velocity vector with measured angle data by a seeker. Relative position and velocity between the target and the observer platform with LOS and LOS rate are main states of the estimation.

Cartesian coordinates and Modified Spherical coordinates (MSC) are explained in details. Moreover, dynamic target model is introduced. Thereafter, observability problems in the angle only target tracking are investigated. At the end of this chapter, different platform maneuvers to obtain observability are analyzed.

2.1 Coordinate Systems

2.1.1 Cartesian Coordinate System

A general choice of coordinate system in the angle-only target tracking problem is to use Cartesian coordinates illustrated in Figure 2.1-1. The x-axis points through the east, the y-axis points through the north.

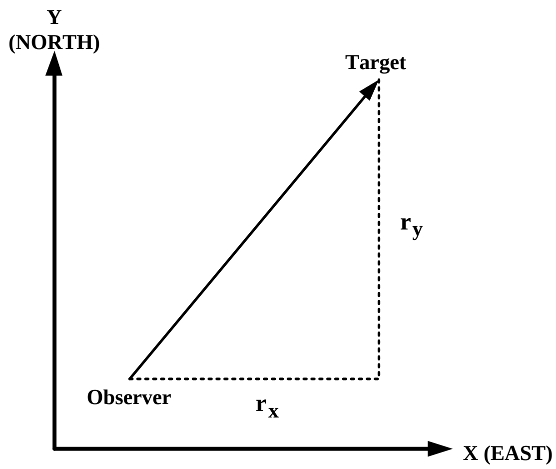

Figure 2.1-1 2D Cartesian Coordinates

The state vector in Cartesian coordinates is denoted by x_{car} and is given by;

$$x_{car} = \begin{bmatrix} x_1 \\ x_2 \\ x_3 \\ x_4 \end{bmatrix} = \begin{bmatrix} x \\ y \\ \dot{x} \\ \dot{y} \end{bmatrix} \tag{0.1}$$

2.1.2 Modified Spherical Coordinate System

Another coordinate system alternative to the Cartesian coordinates is Modified Spherical coordinates (MSC). The state vector in MSC is

$$y_{msc} = \begin{bmatrix} y_1 \\ y_2 \\ y_3 \\ y_4 \end{bmatrix} = \begin{bmatrix} \frac{1}{r} \\ \lambda \\ \frac{\dot{r}}{r} \\ \dot{\lambda} \end{bmatrix} \tag{0.2}$$

The first state is the reciprocal of range, the second state is bearing angle (λ), the third state is range rate divided by range and the fourth state is bearing rate $(\dot{\lambda})$.

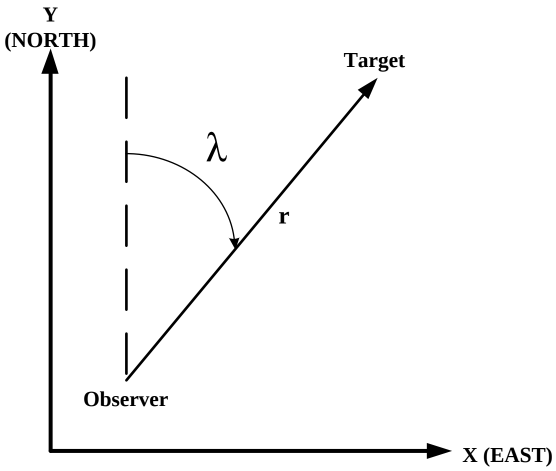

Figure 2.1-2 2D Modified Spherical Coordinates (MSC).

In Figure 2.1-2, r denotes the range between target and observer. λ is the line of sight angle (LOS) and it is measured in the Cartesian coordinates of which the Y-axis is along the initial LOS to the target so that $\lambda(0) = 0$

After searching literature, Cartesian coordinate based extended Kalman filter reveals unstable behavior and biased estimates through the angle-only target tracking problem [6]. Thus, MSC is used to deal with instability and biased estimation. The most important reason to use MSC as coordinate system in the angle-only target tracking is because MSC de-couples observable and unobservable components of the state vector. Even if filter is not fully observable, estimation performance of observable states do not get affected from the unobservable states.

2.2 Dynamic Target Model

Consider a general dynamic model written in the state space form as follows

$$\dot{x} = f_{continuous}(\mathrm{x(t), u(t), w(t)}) \tag{0.3}$$

where x(t) is the state of the system for example range and range rate divided by range. u (t) is input to the system for example observer's maneuver (acceleration of the observer in North-East frame). w (t) is process noise of the system since the target motion is not known perfectly. Target model is needed to be discretized to work with computers. The dynamic target model can be written in discrete time

$$x_{k+1} = f_{discrete}(\mathrm{x}_k, \mathrm{u}_k, \mathrm{w}_k) \tag{0.4}$$

Linear form of dynamic model equations can be written as

$$x_{k+1} = Ax_k + Bu_k + Bw_k \tag{0.5}$$

2.2.1 Constant Velocity State Equations

The constant velocity discrete time state equation for system modeled in Cartesian coordinates is described as below.

$$x_{k+1}^{car} = A_k x_k^{car} + G_k w_k \tag{0.6}$$

$$x_{k+1}^{car} = \begin{bmatrix} 1 & 0 & T & 0 \\ 0 & 1 & T & 0 \\ 0 & 0 & 1 & 0 \\ 0 & 0 & 0 & 1 \end{bmatrix} x_k^{car} + \begin{bmatrix} \frac{T^2}{2} & 0 \\ 0 & \frac{T^2}{2} \\ T & 0 \\ 0 & T \end{bmatrix} w_k \tag{0.7}$$

Bearing angle and bearing rate are measurement of the system and they are written as

$$z_k^{car} = \begin{bmatrix} \lambda \\ \dot{\lambda} \end{bmatrix} = \begin{bmatrix} \arctan\left(\frac{x}{y}\right) \\ \frac{\dot{x}y - x\dot{y}}{x^2 + y^2} \end{bmatrix} \tag{0.8}$$

In Cartesian coordinates, the state equations are linear and time invariant. However, measurement equations are highly nonlinear.

In MSC the continuous state equation of motion can be written as [6]

$$\begin{aligned} \dot{y}_1 &= -y_3 y_1 \\ \dot{y}_2 &= y_4 \\ \dot{y}_3 &= {y_4}^2 - {y_3}^2 + y_1\left[a_x \sin\left(y_2\right) + a_y \cos\left(y_2\right)\right] \\ \dot{y}_4 &= -2 y_4 y_3 + y_1\left[a_x \cos\left(y_2\right) - a_y \sin\left(y_2\right)\right] \end{aligned} \tag{0.9}$$

where a_x and a_y are the Cartesian components of relative acceleration through north and east directions. The detailed derivation of the state equations in MSC can be found in Appendix A.

In the equation set (0.9) under the condition of neither target nor observer maneuver; the last three states are decoupled from the first (inverse of range) state. Therefore, in the absence of acceleration all states except the first is theoretically observable using angle-only information [32].

The measurement equation in MSC is

$$z_k^{msc} = C \cdot \begin{bmatrix} \lambda \\ \dot{\lambda} \end{bmatrix} = \begin{bmatrix} 0 & 1 & 0 & 0 \\ 0 & 0 & 0 & 1 \end{bmatrix} \cdot \begin{bmatrix} \lambda \\ \dot{\lambda} \end{bmatrix} \tag{0.10}$$

2.3 Observability Issue

2.3.1 Observability Analysis

Equation set (0.9) indicates that without any maneuver of the observer (nonzero relative acceleration) y_1 is not observable in the filter if the target is stationary or moving with constant velocity. However, it is stated that in Ref. [14, 30] in the case of nonzero LOS rate, relative range can be estimated for stationary target even if there is no observer maneuver. Thus, for stationary target estimation, proposed filter in Ref. [6] should be modified in such a way that system becomes observable for stationary target without any observer maneuver. This issue is considered as future work and to get observability for both stationary and constant velocity targets, observer executes maneuver through this thesis.

It is mentioned before that in order to obtain full observability; the observer needs to execute a maneuver. When both the observer velocity and target velocity are constant, the a_x and a_y terms are equal to zero, the y_1 term drops off the $\dot{y}_3$ and $\dot{y}_4$ functions. Therefore; y_1 (the reciprocal of range) is not observable when neither the observer nor the target has any acceleration.

Another way to check observability of the system is to check the rank of the observability matrix. If observability matrix is full rank, then all states are observable. The observability matrix is given as

$$O = \begin{bmatrix} C \\ C \cdot A \\ C \cdot A^2 \\ C \cdot A^3 \end{bmatrix} \tag{0.11}$$

where C is the measurement matrix and A is the linearized form of equation set (0.11) and can be shown as

$$A = \begin{bmatrix} \frac{\partial \dot{y}_1}{\partial y_1} & \frac{\partial \dot{y}_1}{\partial y_2} & \frac{\partial \dot{y}_1}{\partial y_3} & \frac{\partial \dot{y}_1}{\partial y_4} \\ \frac{\partial \dot{y}_2}{\partial y_1} & \frac{\partial \dot{y}_2}{\partial y_2} & \frac{\partial \dot{y}_2}{\partial y_3} & \frac{\partial \dot{y}_2}{\partial y_4} \\ \frac{\partial \dot{y}_3}{\partial y_1} & \frac{\partial \dot{y}_3}{\partial y_2} & \frac{\partial \dot{y}_3}{\partial y_3} & \frac{\partial \dot{y}_3}{\partial y_4} \\ \frac{\partial \dot{y}_4}{\partial y_1} & \frac{\partial \dot{y}_4}{\partial y_2} & \frac{\partial \dot{y}_4}{\partial y_3} & \frac{\partial \dot{y}_4}{\partial y_4} \end{bmatrix} \tag{0.12}$$

$$A=\begin{bmatrix} -y_3 & 0 & -y_1 & 0 \\ 0 & 0 & 0 & 1 \\ (a_y + a_x y_2) & y_1(a_x - a_y y_2) & -2y_3 & 2y_4 \\ (a_x - a_y y_2) & -y_1\left(a_x y_2 + a_y\right) & -2y_4 & -2y_3 \end{bmatrix} \qquad (0.13)$$

Observability matrix is a square matrix for a bearing-only (λ is the only measurement for estimation) target tracking problem and observability criterion requires $\det(O) \neq 0$. However, for two measurements (λ and $\dot{\lambda}$), C is a 2x4 matrix and so observability matrix becomes an 8x4 matrix. For multi-measurement systems, although observability matrix is a non-square (n x nm) matrix, $O \cdot O^T$ is square matrix, and thus $\det\left(O \cdot O^T\right) \neq 0$ can be checked for observability.

2.3.2 Observability with Sinusoidal Motion

To get observability through the target tracking estimation problem the observer needs to execute maneuver. First maneuver type studied in this thesis is sinusoidal motion.

Sinusoidal motion can be obtained from open loop $\mp$ acceleration command series or from sinusoidal position command to the observer.

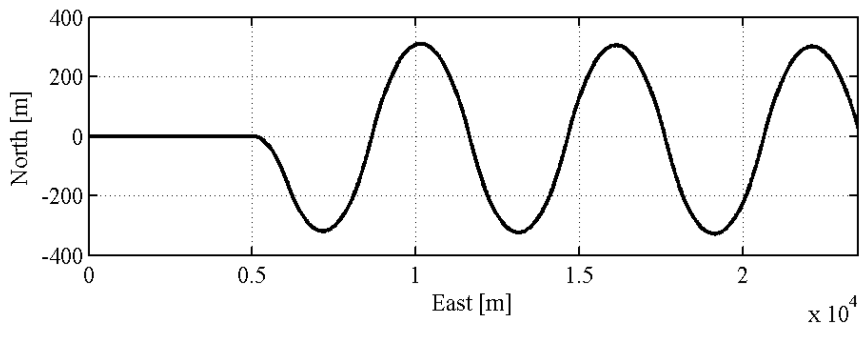

Figure 2.3-1 Sinusoidal motion of the observer

2.3.3 Observability with Modified Proportional Navigation Guidance

Standard proportional navigation guidance law (PNG) does not provide observability for MSC based target state estimation. Another way to obtain observability for target tracking problem is to use modified proportional navigation as guidance law [15, 17, 33]. The missile acceleration command a_c perpendicular to the current LOS generated by MPNG can be expressed for 2D intercept scenarios

$$a_c = NV_c\dot{\lambda} + k\left(\lambda_{current} - \lambda_0\right) \tag{0.14}$$

where N is navigation constant, V_c is closing velocity (V_c can be replaced with missile velocity since ship targets are quite slow compared to the ASMs) and k is a positive constant and should be chosen with consideration of observer maneuver capability. λ_0 is the initial LOS angle where maneuver starts and $\lambda_{current}$ is the current LOS angle measured by the seeker. In the second term of equation (0.14) by subtracting λ_0 from current λ, oscillatory motion is obtained around the initial LOS vector.

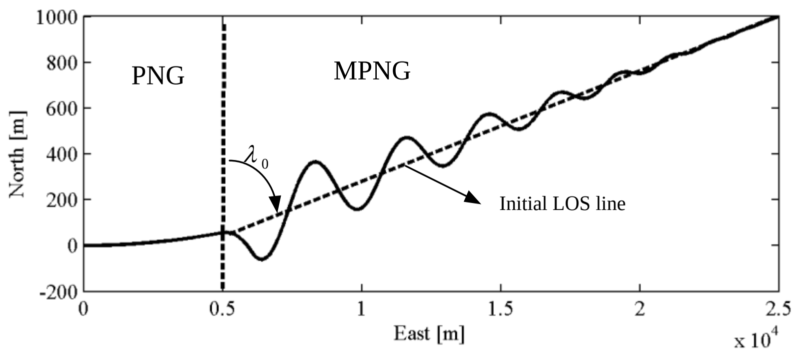

Figure 2.3-2 Missile flight path

The observer is at (0,0) m and the stationary target is at (1,25) km at the beginning of the terminal flight. The observer guided by PNG at first and then guided by MPNG from 0.5 km east to the end of flight.

For the large LOS angles, the second term of equation (0.14) dominates the acceleration command and provides oscillatory motion (helps to increase observability) and then through end of the oscillatory motion second term of guidance law goes to zero. Thus, through end of the flight MPNG becomes PNG and this preserves target hitting efficiency.

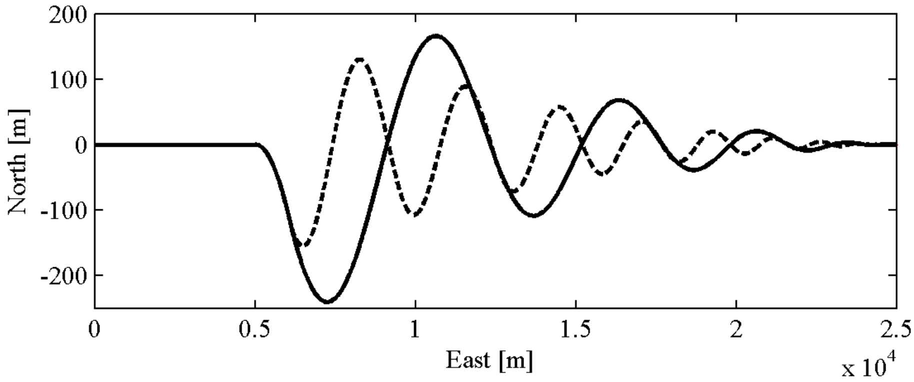

Figure 2.3-3 Observer flight path with MPNG by using different k values

In Figure 2.3-3 observer is at (0, 0) m and target is at (25, 0) km and stationary. If there is no λ from east, modification term of the equation (0.14) is zero and so there will be no oscillatory motion. Because of this, initial heading error (λ) has to be given to the system.

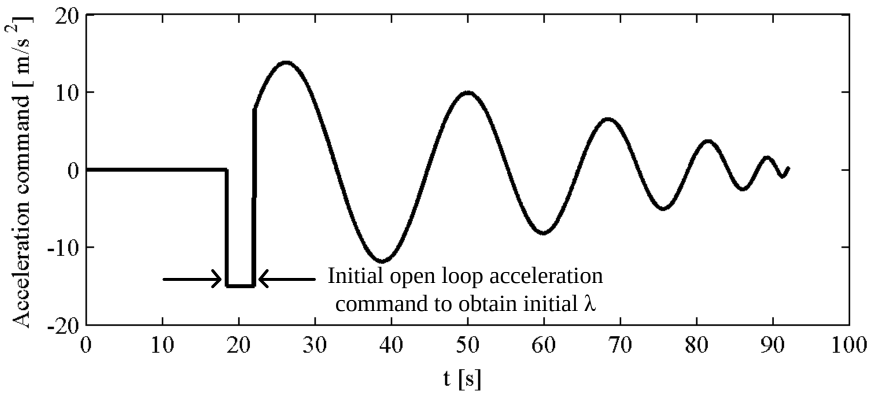

Figure 2.3-4 Acceleration command history for oscillatory observer motion

CHAPTER 3

TRACKING FILTERS

3.1 Used Tracking Filters

3.1.1 Kalman Filter

If dynamic target model, relative states of the system and measurements are taken into account, total system model for angle-only target tracking can be written as

$$\begin{aligned} \mathrm{x}_{\mathrm{k+1}} &= f(\mathrm{x}_k, \mathrm{u}_k, \mathrm{w}_k) \\ \mathrm{y}_k &= c(\mathrm{x}_k, \mathrm{v}_k) \end{aligned} \tag{1.1}$$

where y is measurement vector, x is the state vector and u is the input vector. w and v represent the process and measurement noise respectively and they are assumed to be uncorrelated, zero-mean $\left(i.e.E\left(w_k\right)=E\left(v_k\right)=0\right)$, Gaussian (normal, N) noises with covariance matrices Q_k and R_k respectively.

$$\begin{aligned} w_k &\sim N\left(0, Q_k\right) \\ v_k &\sim N\left(0, R_k\right) \end{aligned} \tag{1.2}$$

For a linear model with noise, the system can be described as

$$x_{k+1} = Ax_k + B_u u_k + B_w w_k \tag{1.3}$$

$$y_k = Cx_k + v_k \tag{1.4}$$

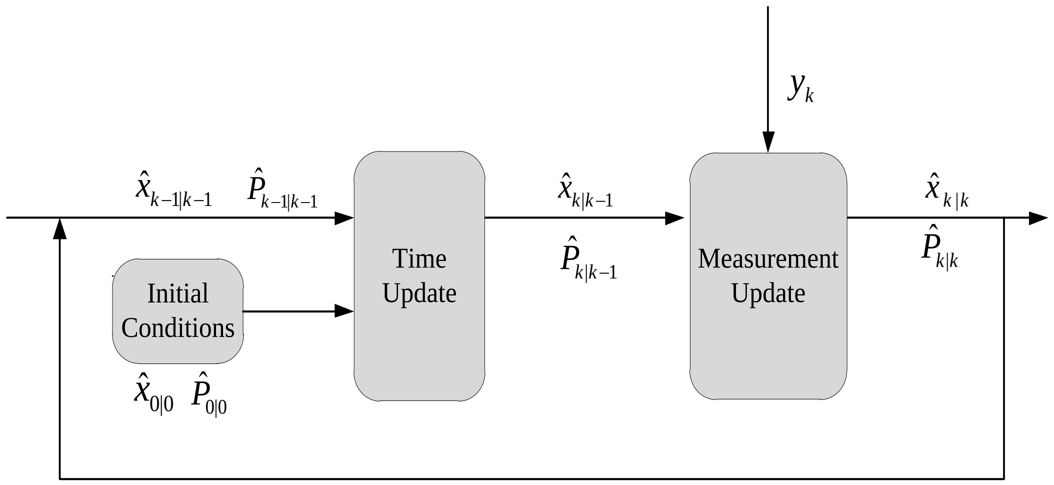

Figure 3.1-1 Kalman filter block diagram

Figure 3.1-1 shows a block diagram of the Kalman filter for one time step. $\hat{x}_{k|k}$ is the estimate of the state vector for time t_k. $\hat{x}_{k|k-1}$ is the estimate of the state vector in time t_{k-1}. $\hat{P}$ is the uncertainty in the estimated state vector and called prediction covariance matrix. Optimal solution of estimation problem of state x based on the measurements y can be obtained by the Kalman filter [34].

Covariance matrix $\hat{P}$ does not depend on measurements. It gives information about how well the filter performs. Kalman gain K determines amount of the innovation term should be included. Large K values means the measurements have great impact on the correction of the estimate. Also, large K values give faster filter that considers the measurements to be reliable. On the other hand, small K values give slower filter which is more robust to measurement noise.

One cycle of Kalman filter algorithm is given below.

Table 3.1-1 One Cycle of Kalman Filter

Time Update $\hat{x}_{k\|k-1} = A\hat{x}_{k-1\|k-1} + Bu_k$ $\hat{P}_{k\|k-1} = A\hat{P}_{k-1\|k-1}A^T + Q_k$ **Measurement Update** $K = \hat{P}_{k\|k-1}C^T\left[C\hat{P}_{k\|k-1}C^T + R_k\right]^{-1}$ $\hat{x}_{k\|k} = \hat{x}_{k\|k-1} + K\left[y_k - C\hat{x}_{k\|k-1}\right]$ $\hat{P}_{k\|k} = \hat{P}_{k\|k-1} - KC\hat{P}_{k\|k-1}$

3.1.2 Extended Kalman Filter

In the case of nonlinear model or measurement equation like in (1.1) an Extended Kalman Filter (EKF) can be used. The idea is to linearize the system and apply a Kalman filter. The EKF equations are given below and the main difference is that the matrices A and C have been replaced with the Jacobians of the functions f and c in the update of $\hat{P}$.

J_f and J_c are the Jacobeans of the functions f and c respectively and their derivations can be found in the Appendix A.

Table 3.1-2 One Cycle of Extended Kalman Filter

Time Update $\hat{x}_{k\|k-1} = f(\hat{x}_k, \mathrm{u}_k, \mathrm{w}_k)$ $\hat{P}_{k\|k-1} = J_f \hat{P}_{k-1\|k-1} J_f^T + Q_k$ **Measurement Update** $K = \hat{P}_{k\|k-1} J_c^T \left[J_c \hat{P}_{k\|k-1} J_c^T + R_k \right]^{-1}$ $\hat{x}_{k\|k} = \hat{x}_{k\|k-1} + K\left[y_k - c(\hat{x}_{k\|k-1}) \right]$ $\hat{P}_{k\|k} = \hat{P}_{k\|k-1} - KJ_c \hat{P}_{k\|k-1}$

3.1.3 Neural Extended Kalman Filter

The neural extended Kalman filter (NEKF) is an estimation procedure that can be used in target tracking systems due to its adaptive nature [26]. When highly nonlinear systems are linearized and discretized or due to mismodeling of system, the plant model may not be totally known [19]. When such conditions occur, estimation of the target states can become insufficient. Using NEKF instead of standard EKF, better estimation results are obtained because NEKF compensates for the unmodelled dynamics of the plant by learning online.

As mentioned in Ref. [20], a neural network can be trained with Kalman filter gains because the neural network weights are coupled to the standard EKF with the state coupling function. The neural network weights are treated as augmented states to the target track.

Given the true system model defined by the nonlinear vector equation

$$x_{k+1} = f\left(x_k, u_k\right) \tag{1.5}$$

and estimator's view defined by the 'hat' system

$$\hat{x}_{k+1} = \hat{f}\left(\hat{x}_k, u_k\right) \tag{1.6}$$

The error between true and estimated system

$$\varepsilon = f - \hat{f} \tag{1.7}$$

can be estimated by artificial neural network. Multi-layer perceptron is used as artificial neural network in this thesis. The multilayer perceptron consists of three or more layers (an input and an output layer with one or more hidden layers). A multilayer perceptron with a single hidden layer (which is used in this thesis) scheme is shown below.

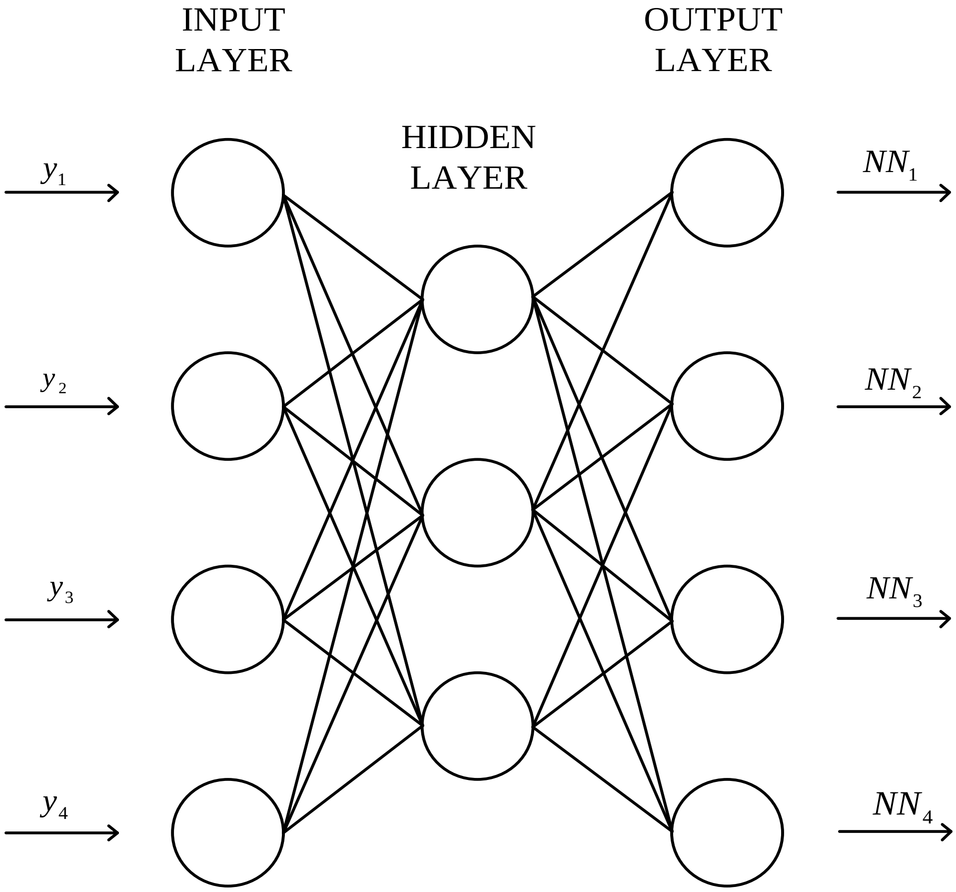

Figure 3.1-2 Used artificial neural network scheme for MLP

Used artificial neural network scheme for MLP with a single hidden layer is given in Figure 3.1-2. There are 4 neurons in input and output layers. Also there are 3 neurons in hidden layer. y_1 y_2 y_3 and y_4 are the states of the MSC-EKF.

After neural network modification, system becomes

$$f = \hat{f} + NN \tag{1.8}$$

In the hidden layer of neural network, a large variety of functions can be used. The function usually used in the NEKF is

$$g(y) = \frac{1 - e^{-y}}{1 + e^{-y}} \tag{1.9}$$

Given activation function in equation (3.9) can squeeze large magnitude values between ∓ 1. It is used as squashing function and shown in Figure 3.1-3.

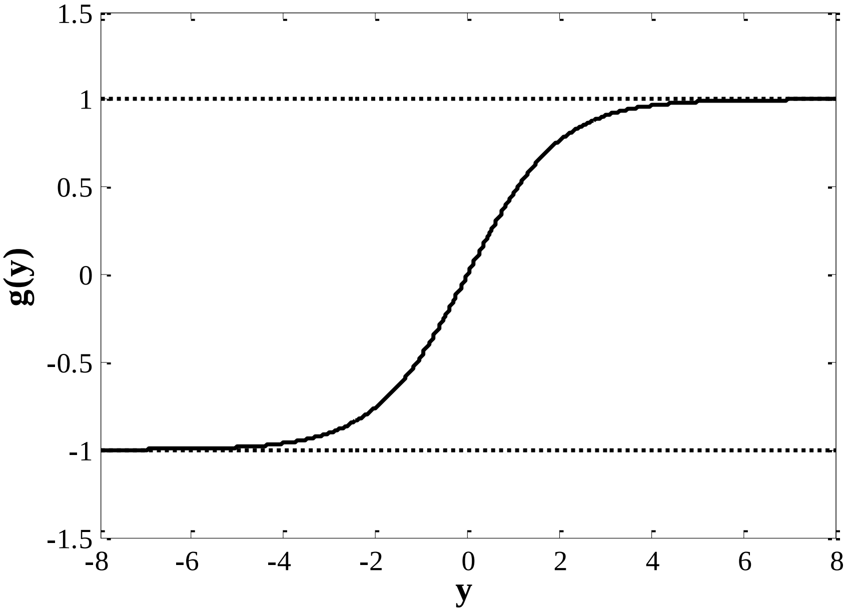

Figure 3.1-3 Sigmoid squashing function used by the neural network in the NEKF

Each output of the artificial neural network which includes the squashing function can be written as

$$NN_{k=1:4}(\mathrm{x}, w, \beta) = \sum_{j=1}^{3} \beta_{jk}\, g\left(\sum_{i=1}^{4} w_{ij} x_i \right) \tag{1.10}$$

where $\mathrm{x_i}$'s are the input signals to the neural network, in this case the estimated states, the function 'g' is defined as squashing function before, w and β are the input and output weights of the neural network respectively. 'i' is the number of neurons in input layer (4 in this case), 'j' is the number of neurons in hidden layer (3 in this case), 'k' is the number of neurons in output layer (4 in this case). Input, output and hidden layer scheme was shown before in Figure 3.1-2.

The neural extended Kalman filter is a combination of the standard extended Kalman and neural network weights, NEKF state vector is

$$\overline{x}_k = \begin{bmatrix} x_k & w_k & \beta_k \end{bmatrix}^T \tag{1.11}$$

There are 4 EKF states, 12 input weights and 12 output weights in the NEKF algorithm in this case and there are 28 states totally.

After including the artificial neural network terms to the system equations explained in chapter 2.2.1, the implemented neural model for the tracking system component of the NEKF becomes

$$f(x_k, u_k) = \hat{f}(\hat{x}_k, u_k) + NN(\hat{x}_k, w_k, \beta_k) = \hat{f}(\hat{x}_k, u_k) + \begin{bmatrix} NN_1(\hat{\mathrm{x}}_k, \mathrm{w}_k, \beta_k) \\ NN_2(\hat{\mathrm{x}}_k, \mathrm{w}_k, \beta_k) \\ NN_3(\hat{\mathrm{x}}_k, \mathrm{w}_k, \beta_k) \\ NN_4(\hat{\mathrm{x}}_k, \mathrm{w}_k, \beta_k) \end{bmatrix} \tag{1.12}$$

In MSC the continuous state equation of motion was written as

$$\begin{aligned} \dot{y}_1 &= -y_3 y_1 \\ \dot{y}_2 &= y_4 \\ \dot{y}_3 &= {y_4}^2 - {y_3}^2 + y_1\left[a_x \sin(y_2) + a_y \cos(y_2)\right] \\ \dot{y}_4 &= -2 y_4 y_3 + y_1\left[a_x \cos(y_2) - a_y \sin(y_2)\right] \end{aligned} \tag{1.13}$$

and the linearized form of these equation set was named A matrix and again it is shown below.

$$A = \begin{bmatrix} -y_3 & 0 & -y_1 & 0 \\ 0 & 0 & 0 & 1 \\ (a_y + a_x y_2) & y_1(a_x - a_y y_2) & -2y_3 & 2y_4 \\ (a_x - a_y y_2) & -y_1\left(a_x y_2 + a_y\right) & -2y_4 & -2y_3 \end{bmatrix} \tag{1.14}$$

Then the discretized form of the A matrix is

$$\overline{A} = A \cdot dt + I \tag{1.15}$$

where dt is the sampling time.

The associated Jacobian of the NEKF for target tracking would be

$$\bar{J}_f = \frac{\partial f(\bar{x}_k)}{\partial \bar{x}_k} = \begin{bmatrix} \left[\underbrace{\bar{A} + \frac{\partial NN(x_k, w_k, \beta_k)}{\partial x_k}}_{4x4} \right] & \left[\underbrace{\frac{\partial NN(x_k, w_k, \beta_k)}{\partial w_k}}_{4x12} \quad \underbrace{\frac{\partial NN(x_k, w_k, \beta_k)}{\partial \beta_k}}_{4x12} \right] \\ \left[\underset{24x4}{0} \right] & \left[\underset{24x24}{I} \right] \end{bmatrix} \quad (1.16)$$

Equation (1.16) results in the state estimation and neural network training being coupled. Using these equations as the system dynamics, the equations of the NEKF are written as

$$\hat{\bar{x}}_{k|k-1} = \begin{bmatrix} \hat{x}_{k|k-1} \\ \hat{w}_{k|k-1} \\ \hat{\beta}_{k|k-1} \end{bmatrix} = \begin{bmatrix} f\left(\hat{x}_{k-1|k-1}, u_{k-1}\right) + NN\left(\hat{x}_{k-1|k-1}, \hat{w}_{k-1|k-1}, \hat{\beta}_{k-1|k-1}\right) \\ \hat{w}_{k-1|k-1} \\ \hat{\beta}_{k-1|k-1} \end{bmatrix} \quad (1.17)$$

$$\hat{P}_{k|k-1} = \bar{J}_f \hat{P}_{k-1|k-1} \bar{J}_f^T + Q_k \quad (1.18)$$

$$K = \hat{P}_{k|k-1} C^T \left[C \hat{P}_{k|k-1} C^T + R \right]^{-1} \quad (1.19)$$

$$\hat{\bar{x}}_{k|k} = \begin{bmatrix} \hat{x}_{k|k} \\ \hat{w}_{k|k} \\ \hat{\beta}_{k|k} \end{bmatrix} = \hat{\bar{x}}_{k|k-1} + K\left[y_k - C\hat{\bar{x}}_{k|k-1} \right] \quad (1.20)$$

$$\hat{P}_{k|k} = \left[I - KC \right] \hat{P}_{k|k-1} \quad (1.21)$$

and for MSC target tracking problem, the measurement matrix in the above equation set to handle the change in dimensionality becomes

$$C = \begin{bmatrix} 0 & 1 & 0 & 0 & \\ & & & & 0_{2x24} \\ 0 & 0 & 0 & 1 & \end{bmatrix} \tag{1.22}$$

3.2 Implementation of the EKF

Two filters have been implemented in Matlab environment, an EKF and a NEKF with MSC for tracking non-maneuvering targets. This chapter discusses the initialization of the EKF and NEKF.

3.2.1 Initialization of the State Vector

Let V_{mis} be the velocity vector of the missile and V_{tar} be the velocity vector of the target. The magnitude of the velocities are denoted as v_{mis} and v_{tar} respectively. The missile flies through the x-axes and detects the target at the distance r_{init} . The mentioned simple scenario demonstrated in Figure 3.2-1.

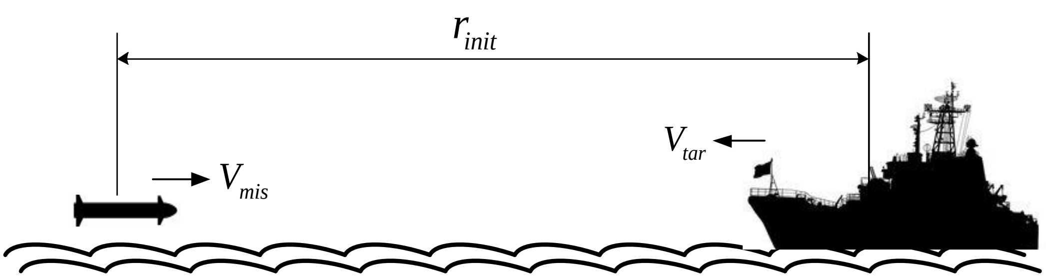

Figure 3.2-1 Initial missile-target position and velocity vectors

The state vector is initialized with a guess of the initial position and velocity of the target in MSC. To initialize the LOS and LOS rate of the system, the first measurements of LOS and LOS rate are used. To include the effect of initial error in range, the range is initialized with $r_{init} + \Delta r$ where Δr is the error in initial range. In the same way, initial relative speed is initialized with $v_{mis} + \Delta v$ since the target speed is quite small compared to the missile. The initial state vector becomes

$$y_{init} = \begin{bmatrix} \dfrac{1}{r_{init} + \Delta r} & \lambda_{meas} & -\dfrac{v_{mis} + \Delta v}{r_{init} + \Delta r} & \dot{\lambda}_{meas} \end{bmatrix}^T \tag{1.23}$$

3.2.2 Initialization of $\hat{P}$

Detailed explanation for covariance matrix initialization can be found in Ref. [1, 30, 31]. Then, initialization of the prediction covariance matrix is

$$\hat{P}_{init} = diag\left(\begin{bmatrix} \dfrac{\sigma_r}{r_{init}^2} & \sigma_\lambda & \dfrac{\sigma_{\dot{r}}}{r_{init}} & \sigma_{\dot{\lambda}} \end{bmatrix}\right)^2 \tag{1.24}$$

where σ_r is standard deviation of range, σ_λ and $\sigma_{\dot{\lambda}}$ are standard deviation of LOS and LOS rate respectively. $\sigma_{\dot{r}}$ is the standard deviation of range rate.

3.2.3 Process Noise Q and the Measurement Noise R

The uncertainty in state estimation due to random target dynamics or mismodeling of target dynamics is typically represented by the process noise covariance matrix Q [3]. Consider the constant velocity (CV) target model in which target acceleration is modeled as white noise

$$a_x(\mathrm{t}) = w(\mathrm{t}) \tag{1.25}$$

where the white noise process $w(\mathrm{t})$ is defined by

$$\begin{aligned} &E[\mathrm{w(t)}] = 0 \\ &E[\mathrm{w(t)\,w(}\tau)] = \mathrm{q(t)}\delta(\mathrm{t}-\tau) \end{aligned} \tag{1.26}$$

The resulting process noise covariance matrix, for states $\begin{bmatrix} x & \dot{x} \end{bmatrix}^T$, becomes

$$Q = \begin{bmatrix} \frac{T^3}{3} & \frac{T^2}{2} \\ \frac{T^2}{2} & T \end{bmatrix} \sigma_q^2 \qquad (1.27)$$

where T is sampling interval and σ_q is the target maneuver standard deviation. The choice of σ_q can be considered as tuning process for simulation results. For the states $\begin{bmatrix} x & y & \dot{x} & \dot{y} \end{bmatrix}^T$ process noise covariance matrix becomes in Cartesian coordinates

$$Q = \begin{bmatrix} \frac{T^3}{3} & 0 & \frac{T^2}{2} & 0 \\ 0 & \frac{T^3}{3} & 0 & \frac{T^2}{2} \\ \frac{T^2}{2} & 0 & T & 0 \\ 0 & \frac{T^2}{2} & 0 & T \end{bmatrix} \sigma_q^2 \qquad (1.28)$$

Q is formulated in Cartesian coordinates but tracking filter completed in MSC. To express process noise in MSC, necessary transformation of Q from Cartesian to MSC is derived in Appendix A.

The measurement noise in LOS and LOS rate are assumed to be independent. R is a diagonal matrix which is given below.

$$R = diag\left(\sigma_\lambda^2 \quad \sigma_{\dot{\lambda}}^2\right) \qquad (1.29)$$

where σ_λ and $\sigma_{\dot{\lambda}}$ are the standard deviation of the measurement noise.

3.3 Implementation of the NEKF

Since NEKF is the combination of EKF and artificial neural network weights, target related state vector and covariance matrix are initialized in the same way as EKF. Weights and weights covariance matrix are initialized with the same scale of other states and covariance values.

CHAPTER 4

SIMULATION AND DISCUSSION

4.1 Used Filter Parameter Values

In this chapter, the results from the performed simulations for target tracking problem with NEKF and EKF are given. As mentioned earlier, the filters are designed for non-maneuvering targets. Before giving the results, parameters needed to be set to initialize the given filters. The first parameter is the initial range.

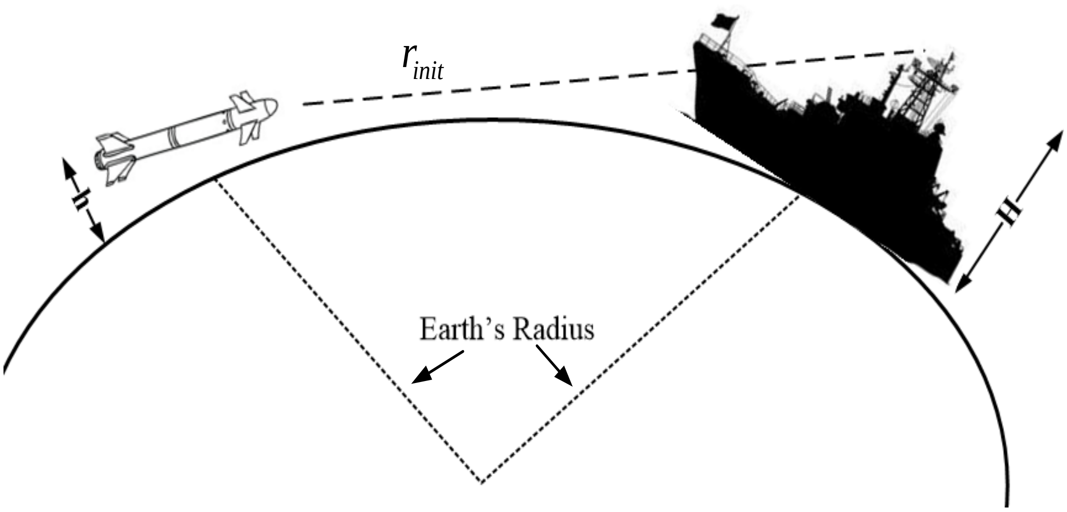

Figure 4.1-1 The moment when the target detects the missile

For the scenario in Figure 4.1-1, missile cruise height h is 5 meters and the ship's radar antenna is about 50 meters over the sea. And also earth radius r_e is taken as 6,371 km. With the help of simple geometry, first missile detection by the radar is calculated as follows

$$r_{init} = \sqrt{(r_e + H)^2 - (r_e + h)^2} \cong 24000m \qquad (2.1)$$

Throughout this chapter; initial range for the simulation scenarios is taken as 24000 m. Speed of missile is taken as 272 m/s and if the target is not stationary its speed is taken as 30 m/s. Standard deviation of LOS angle measurement noise is 0.6 degree and standard deviation of LOS rate measurement noise is 0.015 degree/seconds. Initial estimate of range standard deviation σ_r is 2000 m and standard deviation for target speed is taken as 10 m/s. Sampling rate T is 0.01 s. Standard deviation of the EKF process noise σ_q is taken as 0.01 m/s^2. For the NEKF, initial values of the weights are taken as 0.0001 and standard deviations of the weights are $10^{-10} I$.

4.2 Estimation with Sinusoidal Motion

4.2.1 Stationary Target

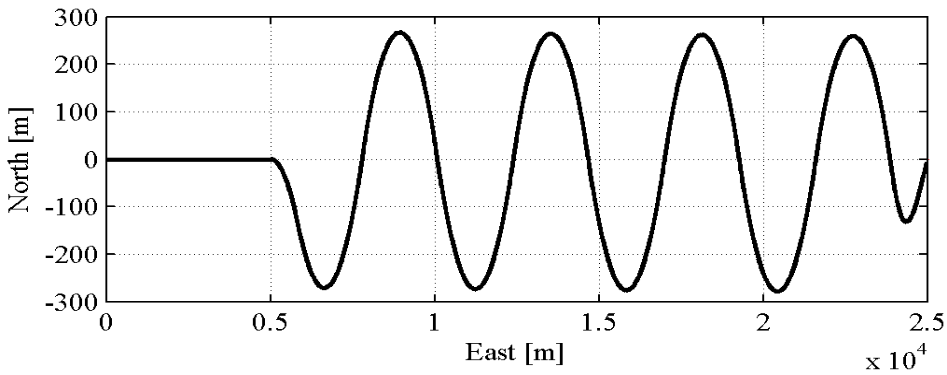

Figure 4.2-1 Missile flight path

In this scenario, missile is at (0,0) and the target is stationary at (25,0) km. The missile is guided by PNG between (0,0) and (0.5,0) km. Then it starts sinusoidal motion by open-loop acceleration commands and this motion ends until 1 km to the stationary target. In the last 1 km, the missile is guided by PNG. Estimation of the range is carried out through the sinusoidal motion.

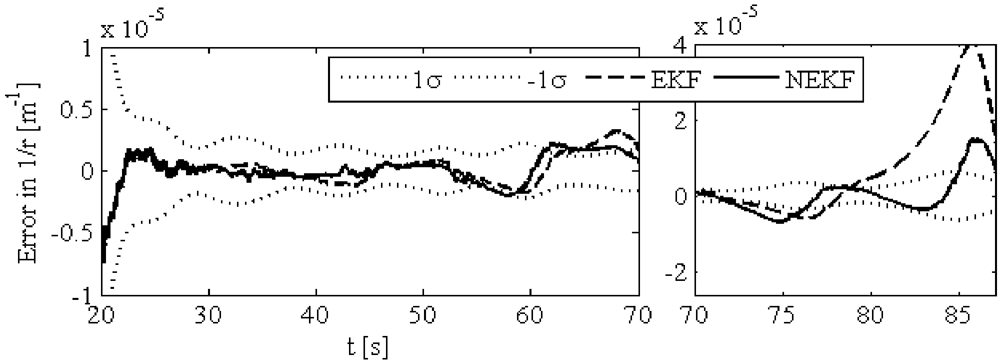

Figure 4.2-2 Estimation error in 1/r

Figure 4.2-2 shows the estimation error in 1/r. Because of the scaling issue, figure is divided into 2 parts, before and after 70th second. The estimation stars at about 20th second.

For a perfectly tuned filter, the error is expected to be out of the covariance bounds about 32 percent of the time (for 1σ) at maximum. In Figure 4.2-2, the estimated range with the NEKF is better than the estimated range with the EKF. Range error is about 24 percent for the EKF and 17 percent for the NEKF and both filters converge to the true value in less than 1 second.

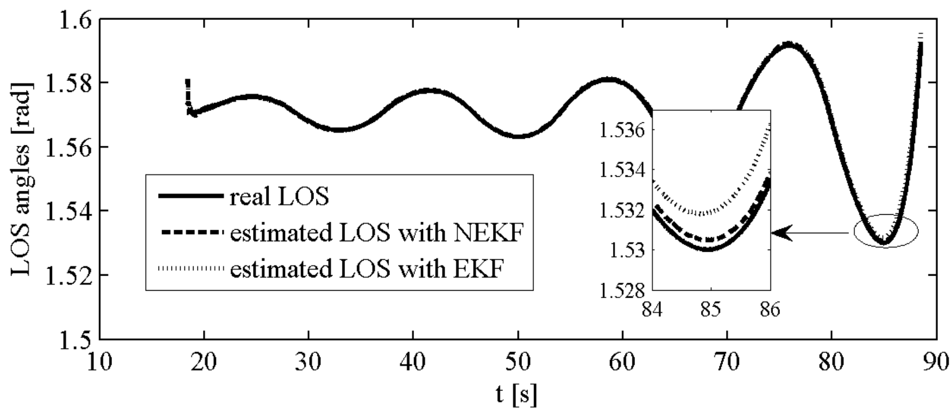

Figure 4.2-3 LOS angles

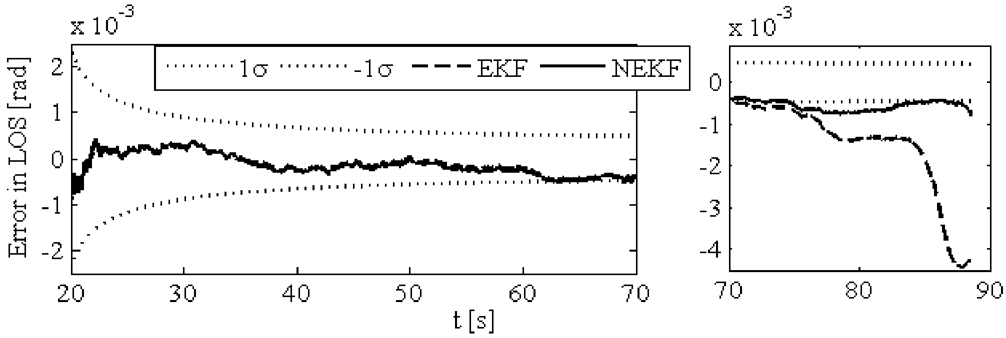

Figure 4.2-4 Error in LOS (λ)

Figure 4.2-3 shows the real and estimated LOS angles. Figure 4.2-4 shows estimation error in λ and it is dived into 2 parts due to the scaling issue. λ is zero at north and in this scenario the missile moves through the east so LOS angle results are around $\pi/2$.

Both EKF and NEKF give the same estimation results between 20th and 70th seconds. After 70th second, the NEKF gives better result than the EKF and both filter errors are less than 32 percent (about 21 percent). This situation stems from the fact that the LOS angle starts to grow through the end of the flight and this growth results with linearization error in the Jacobian matrices. Therefore neural terms of the NEKF increase the filter performance.

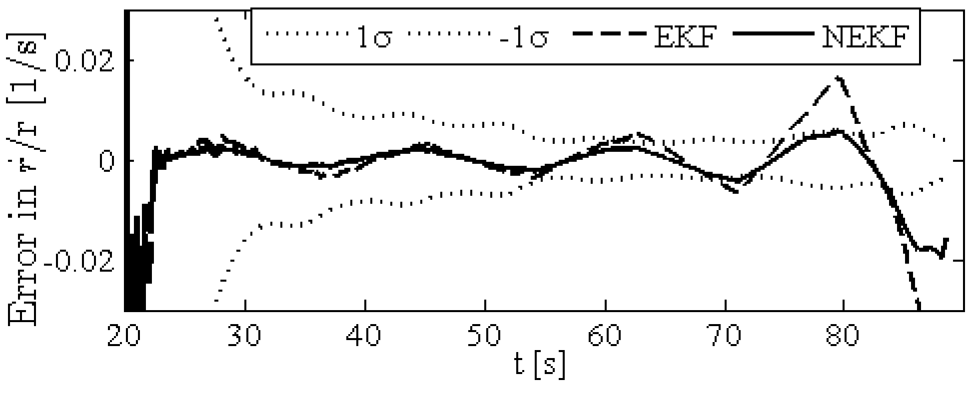

Figure 4.2-5 Error in $\dot{r}/r$

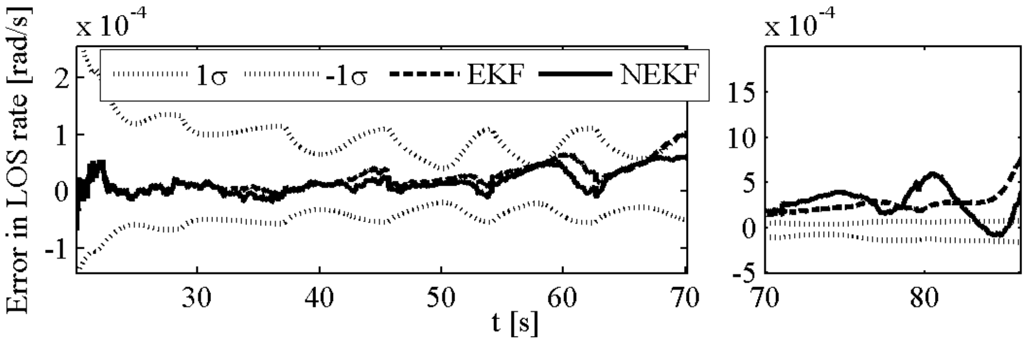

Figure 4.2-6 Error in LOS rate

Figure 4.2-5 shows error in $\dot{r}/r$ and the estimation error for the NEKF is about 9 percent and for the EKF it is about 16 percent. Figure 4.2-6 shows the error in LOS rate estimation and again the NEKF has better filter performance than the EKF.

From the simulation results, the NEKF shows better performance than EKF where the LOS angle starts to grow and linearization based errors in the Jacobian matrices emerges. Basically, the NEKF improves the LOS and LOS rate filtering performance and this enhancement also improves the estimation of the other states.

4.2.2 Constant Velocity Target (CV)

In this scenario, at the beginning the missile is at (0,0) and the target is at (25,0) km. Also the missile has initial 4 degrees heading angle from the east. Target has constant 20 m/s velocity components through the east and north. The missile is guided by PNG until the relative range decreases up to 20 km. Then the missile starts the sinusoidal motion by open-loop acceleration commands and the estimation starts with sinusoidal motion and ends with it. When the estimated relative range is less than 1 km, sinusoidal motion of the missile stops and at last 1 km the missile is guided by PNG again. In Figure 4.2-7, the flights paths of the missile-target and the corresponding interception geometry are demonstrated.

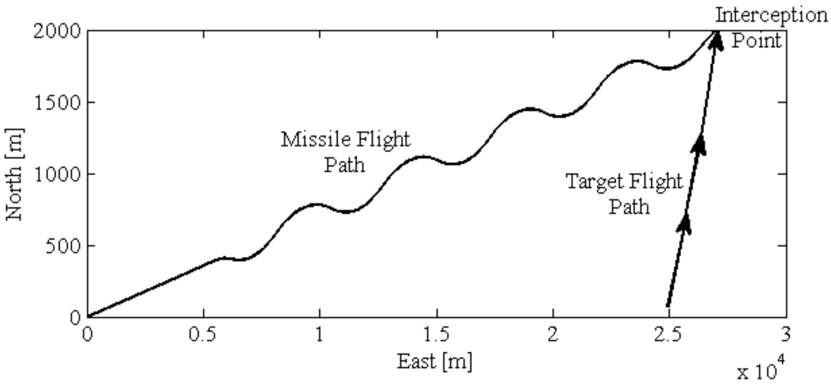

Figure 4.2-7 Missile-target interception geometry

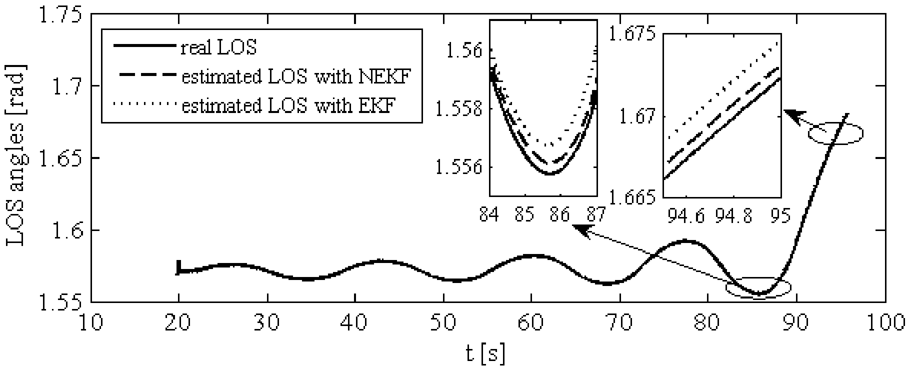

Figure 4.2-8 LOS angles

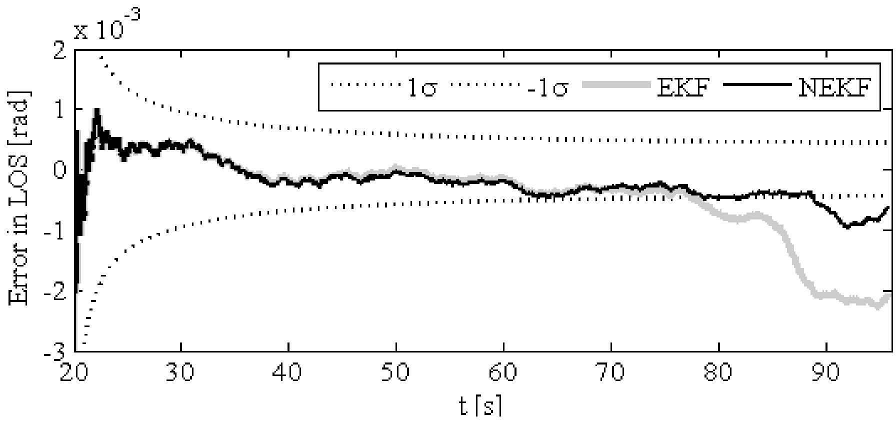

Figure 4.2-9 Error in LOS (λ)

In Figure 4.2-8, estimation starts with the sinusoidal motion at 20th second and ends with the sinusoidal motion similarly. Up to 70th second, the NEKF and the EKF give the same error results. However, after 70th second, the NEKF gives closer value to the real LOS angle than the EKF in Figure 4.2-8. This result is also demonstrated as error covariance in Figure 4.2-9. This is because neural network terms of the NEKF improve the filtering performance.

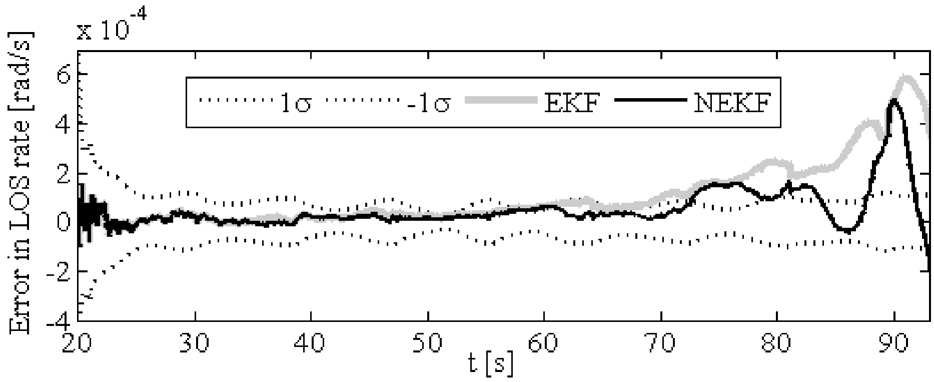

Figure 4.2-10 Error in LOS rate $(\dot{\lambda})$

There is improvement for the estimated LOS rate and error percentage for NEKF is lower than EKF

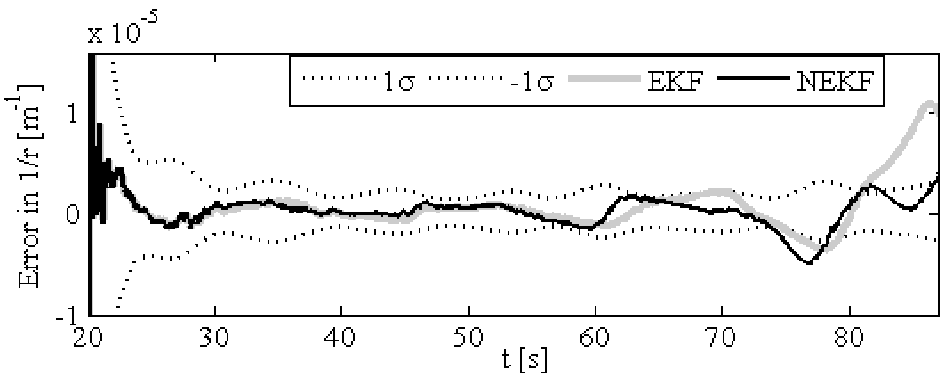

Figure 4.2-11 Error in 1/r

Figure 4.2-11 shows error in reciprocal of range estimation through the sinusoidal motion. Until the 70th second, the NEKF and the EKF give approximately the same results. However, after 70th second, the NEKF gives better result than the EKF, especially at last 10 seconds of the estimation. This is because neural network terms increase the filtering performance of LOS and LOS rate and better measurement data filtering results with better estimation of relative range.

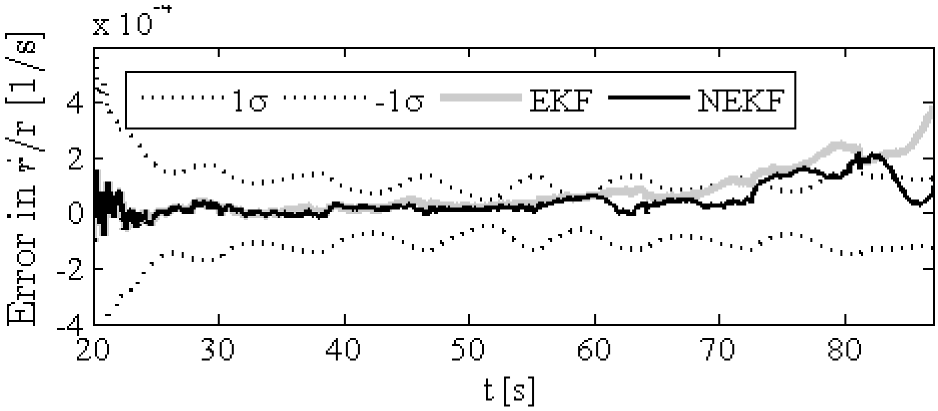

Figure 4.2-12 Error in $\dot{r}/r$

Figure 4.2-12 gives the $\dot{r}/r$ estimation error. The error is around 24 percent for the EKF and 21 percent for the NEKF. This is again reflection of better filtering in LOS and LOS rate.

4.3 Estimation with MPNG

4.3.1 Stationary Target

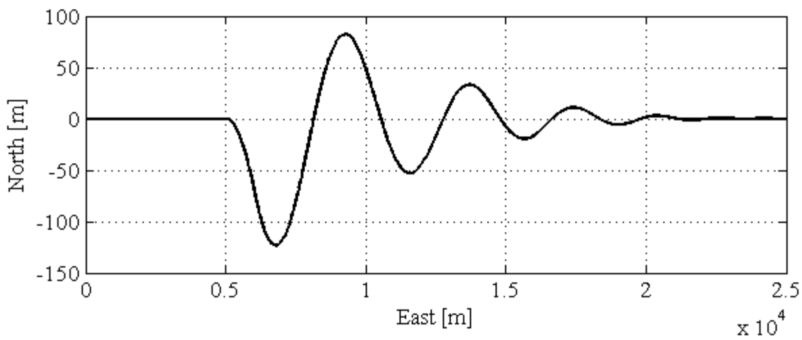

Figure 4.3-1 Missile flight path

In this scenario, the missile is at (0,0) and the target is stationary and situate at (25,0) km. The missile is guided by PNG from the origin to 5 km east. Then, the open-loop acceleration command applied to the missile for 3 seconds to be able to use MPNG rule. Consequently, the missile obtains initial heading angle from the reference east and MPNG can be applied to obtain oscillatory motion to get observability for the range estimation.

The main difference between sinusoidal motion and oscillatory motion by MPNG is acceleration command history for obtaining these motions. For the sinusoidal motion, open-loop acceleration command is applied to the missile through the flight. However, this open-loop command history causes to miss the target if any calculation mistake occurs through the estimation of relative range. On the other hand, oscillatory motion by MNG has closed-loop structure for guidance. Second term of equation (0.14) causes oscillation in the missile flight path to get observability for range estimation. Through the end of the flight, this term begins to become insignificant and MPNG turns into PNG and this feature prevents the missile from the target-miss.

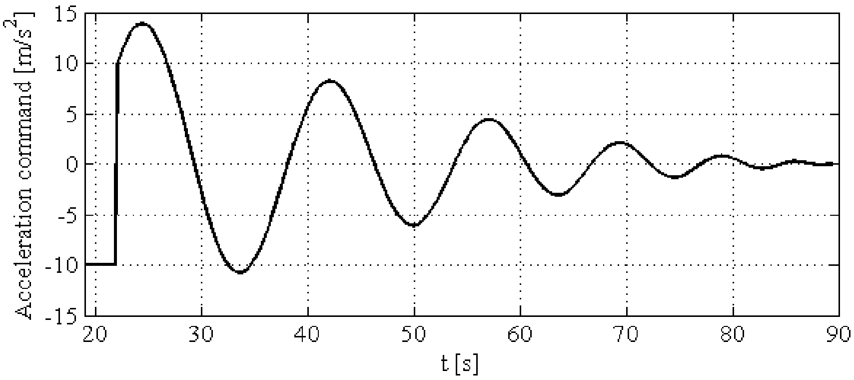

Figure 4.3-2 Missile MPNG acceleration command history for stationary target

As mentioned before in section 4.2 (sinusoidal motion analysis), when the missile becomes closer to the target, the LOS angle starts to increase and it triggers the linearization error in covariance update of the filter. However, the motion obtained by MPNG does not cause the LOS angle increase when the missile is close to the target; hence there is no error or difference is expected between the EKF and the NEKF error covariance graphs for the target state estimation with the motion obtained by MPNG.

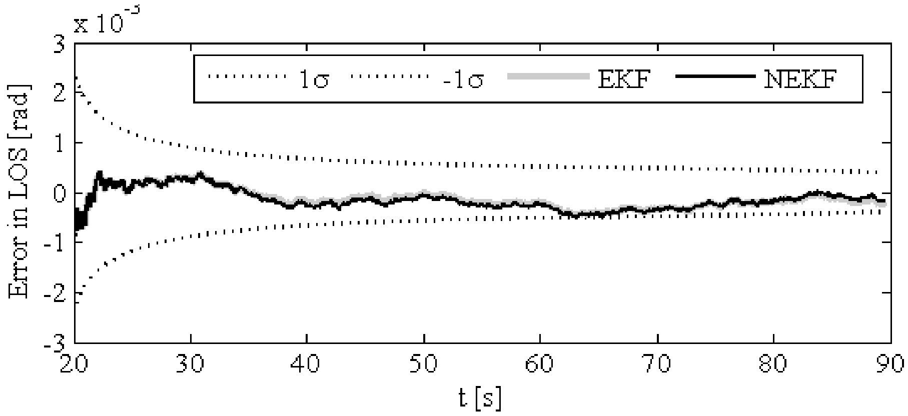

Figure 4.3-3 Error in LOS angle (λ)

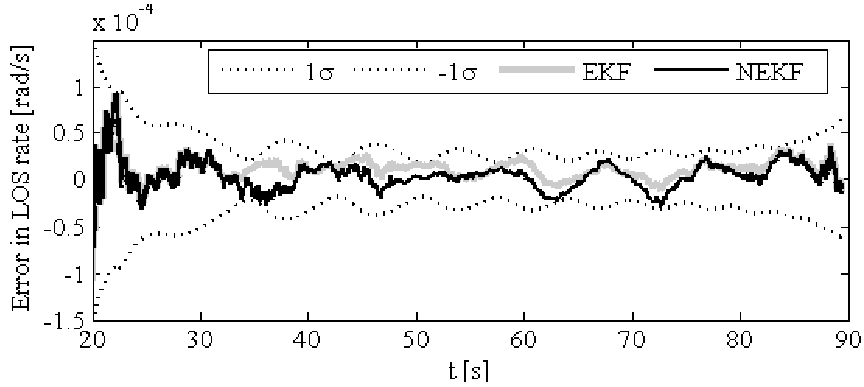

Figure 4.3-4 Error in LOS rate $(\dot{\lambda})$

Figure 4.3-3 and Figure 4.3-4 reveal the results of estimation error in LOS and LOS rate. There is no difference between LOS and LOS rate estimation by the EKF and the NEKF as expected.

Thus far, target state estimation with the flight path obtained by MPNG gives better results than the estimation with flight path obtained by sinusoidal motion of the missile. There is no measurement filtering error in error covariance matrices of the estimation problem for oscillatory motion. This improvement in measurement filtering leads to expecting a better range estimation. However, in Figure 4.3-5 improvement in the range estimation is not apparent. On the contrary, both the EKF and the NEKF start to diverge after about 65th second.

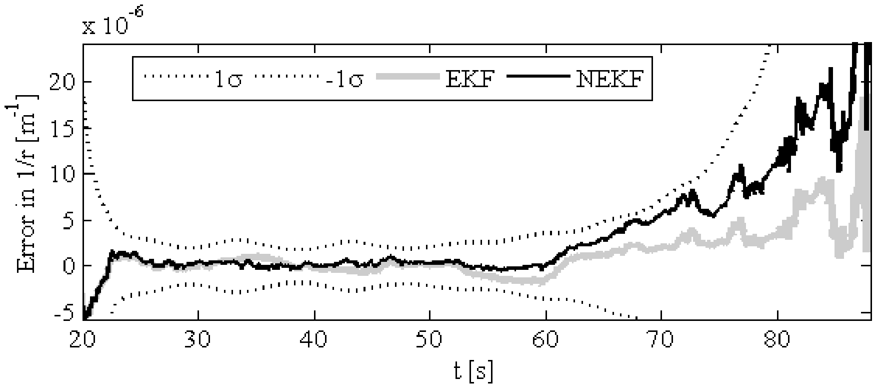

Figure 4.3-5 Error in 1/r

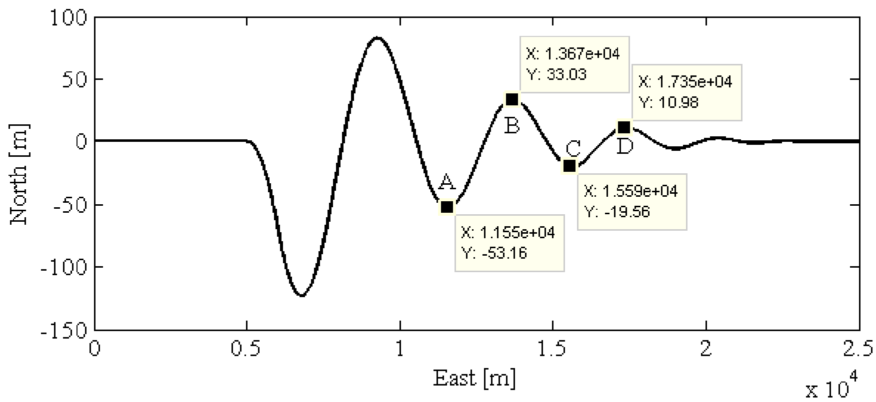

Figure 4.3-6 Detailed missile flight path

Figure 4.3-6 shows the detailed missile flight path. The points A-B-C and D are the peaks of the missile oscillatory flight path. If the relation between Figure 4.3-5 and Figure 4.3-6 is analyzed, it could be interpreted that after the point B, oscillation amplitude of the missile flight path becomes insufficient for the estimation. This insufficiency causes unobservability and unobservable system starts to diverge.

The NEKF has a rapidly increasing covariance error and the error is larger than EKF. The NEKF includes the neural network function into the covariance prediction equation. Without the observability of the target system, the NEKF cannot adequately train its weights. The weights are coupled to the states. Thus, their error growth is also involved in the target track states. In addition, the error covariance cannot be reduced without observability.

This phenomenon can be seen in the estimation of $\dot{r}/r$. Related graph with $\dot{r}/r$ is given in Figure 4.3-7.

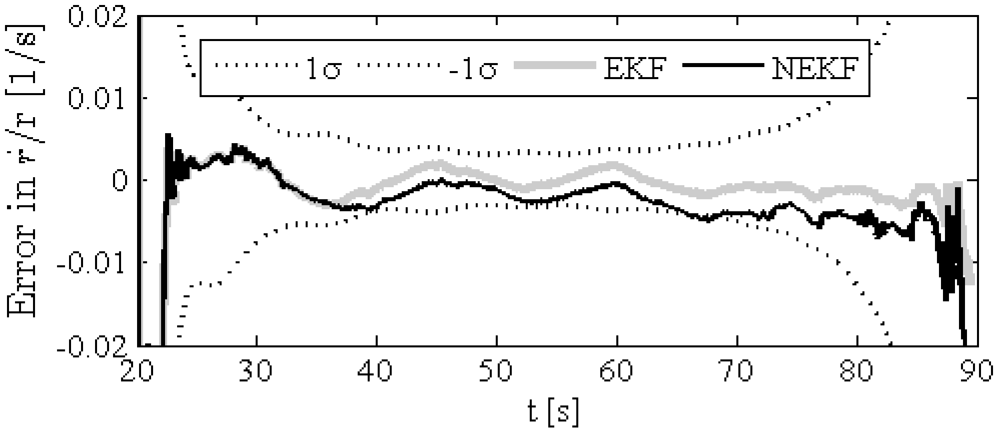

Figure 4.3-7 Error in $\dot{r}/r$

4.3.2 Constant Velocity Target (CV)

In this interception flight geometry, missile is at (0,0) and target is at (25,0) km at the beginning. Target has constant velocity components through the east and north which are 20 m/s for both east and north. In Figure 4.3-8, the missile and the target intercepts at (27,2) km. Until the relative range is 20 km between the missile and the target, the missile is guided with PNG. After that point, guidance law is changed with MPNG to get observability for the range estimation.

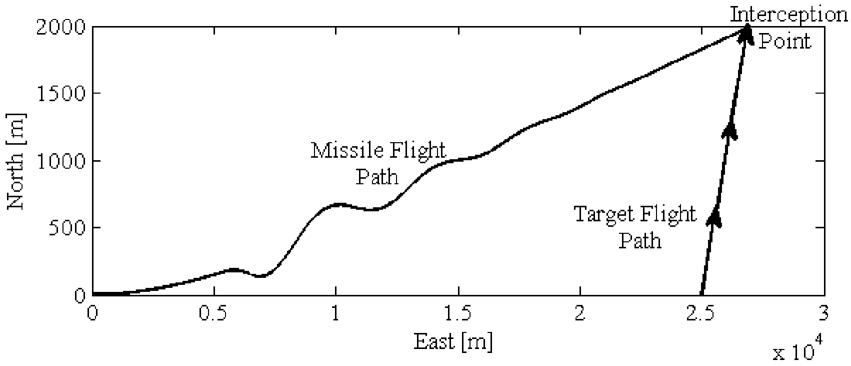

Figure 4.3-8 Missile-target interception geometry

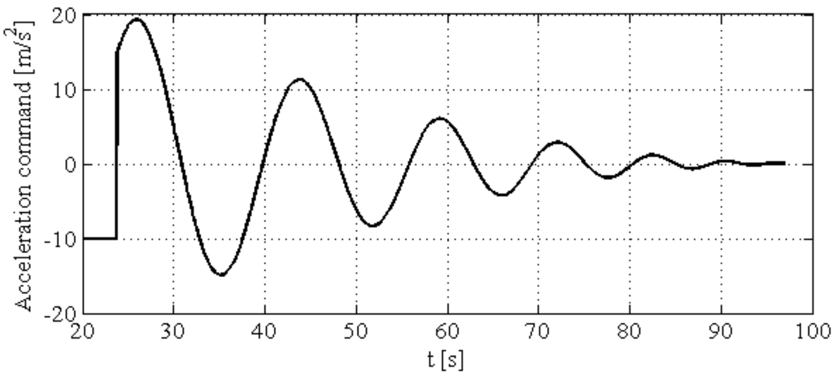

Figure 4.3-9 Missile MPNG acceleration command history for constant velocity (CV) target

Figure 4.3-9 shows missile acceleration command history for constant velocity target interception. This missile acceleration profile is almost the same as missile acceleration profile for stationary target (Figure 4.3-2) because the target velocity is quite small when it is compared with the missile velocity.

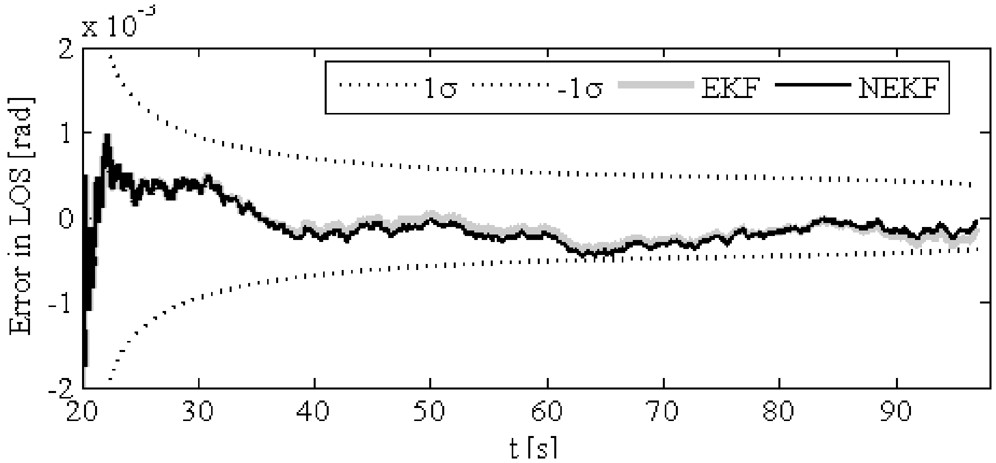

Figure 4.3-10 Error in LOS angle (λ)

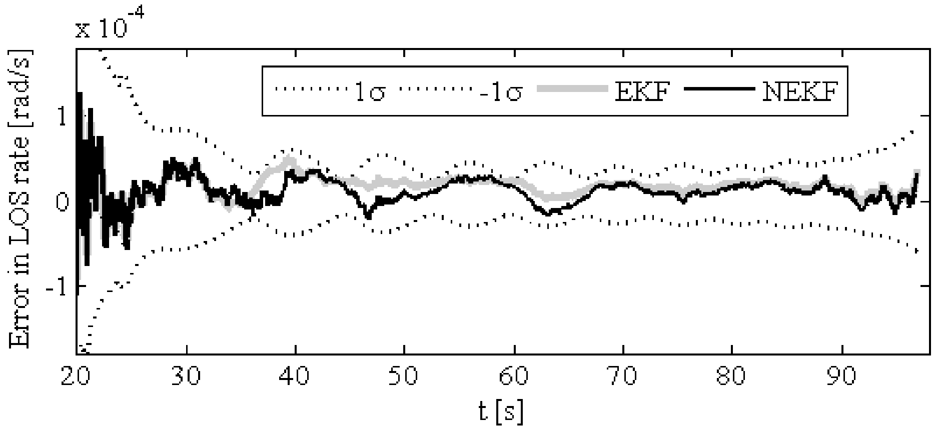

Figure 4.3-11 Error in LOS rate $(\dot{\lambda})$

Figure 4.3-10 and Figure 4.3-11 show error covariance of the LOS angle and the LOS rate respectively. Similar to the stationary target tracking scenario, there is almost no difference between the NEKF and the EKF in terms of filtering the measurements. However, the effect of this improvement is not seen in the state 1/r.

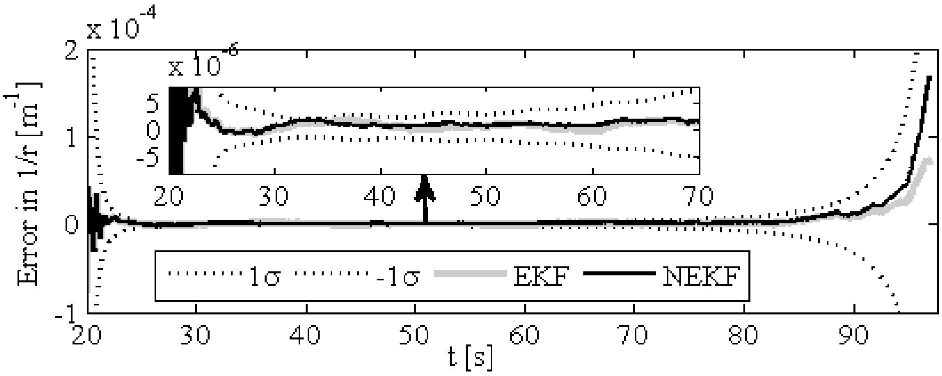

Figure 4.3-12 Error in 1/r

Through the end of the flight, oscillation amplitude of the missile flight path is not sufficient for the target state estimation. Thus, the system becomes unobservable and the unobservable system starts to diverge, consequently.

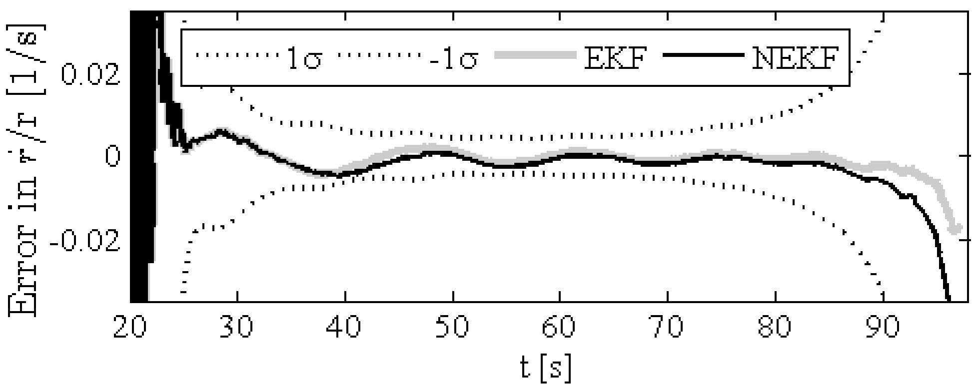

Figure 4.3-13 Error in $\dot{r}/r$

The same divergency is apparent in the error covariance of $\dot{r}/r$. Since with the NEKF the neural terms are included in the covariance update equation and the weights are coupled to the states, the error growth is occurred faster than the EKF for the unobservable case of the estimation.

4.4 Estimation Comparison between Sinusoidal Motion and MPNG

Previously the state estimation of a target was implemented after obtaining observability for the estimation by sinusoidal motion and MPNG. It was obtained that sinusoidal motion is sufficient for observability but through the end of the flight LOS angle starts to increase and this increase causes an error in the LOS angle filtering and this filtering error affects the performance of range estimation. After realizing this problem instead of using the standard EKF, the NEKF is introduced to overcome this problem.

Another maneuver to get the observability for the range estimation is obtained by using modified proportional navigation as guidance law. MPNG is composed of two terms. The first term is the standard proportional navigation guidance and the second term includes LOS angle multiplied with a constant. This second term of the MPNG is the source of the oscillatory motion. With the oscillatory motion estimation, the system becomes observable and through the end of the flight MPNG becomes standard PNG which guarantees the target hit.

There is no LOS angle increase for the maneuver obtained by MPNG. Instead of LOS angle increase, there is reduction in the amplitude of oscillation and this reduction causes LOS angle reduction too. As a result the system becomes unobservable for the estimation and estimation of the range starts to diverge.

In this part the main issue is to analyze the maneuver type studied in this thesis for the range estimation problem. To get the same estimation error covariance for both maneuvers with MPNG and sinusoidal motion, estimation is performed when the system is observable for the MPNG and the LOS angle does not start to increase.

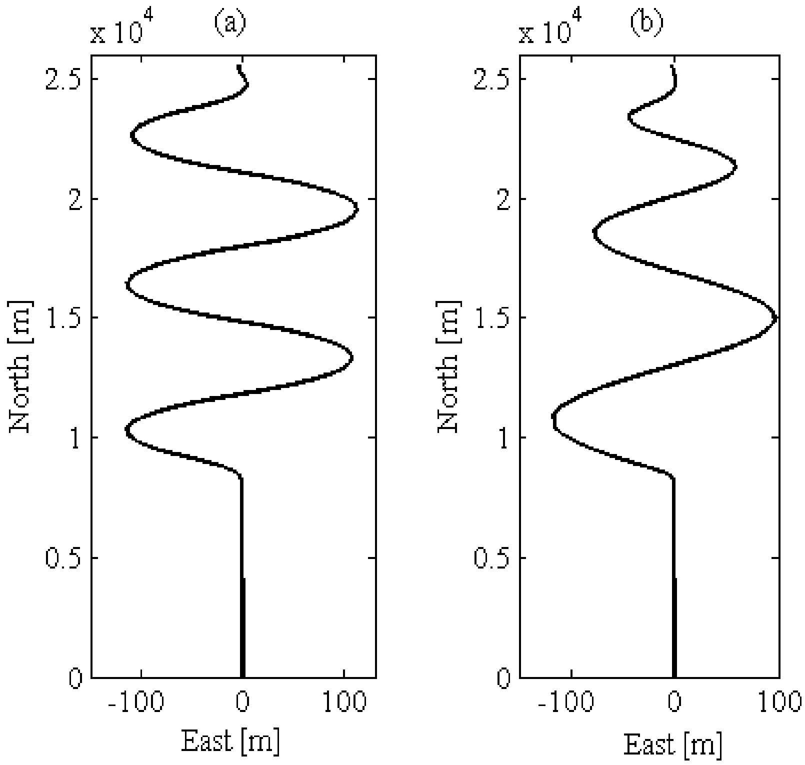

Figure 4.4-1 Flight path of the missile for stationary target, (a) is for sinusoidal motion and (b) is for MPNG

To analyze the effect of maneuver type on estimation performance, two simulation scenarios are generated. In Figure 4.4-1, the missile flight paths are shown. In part (a), maneuver by sinusoidal motion and in part (b) maneuver by MPNG are demonstrated. All conditions for both of the scenarios are the same other than the maneuver types.

As stated earlier, the main purpose of this section is to analyze the effect of the maneuver type for range estimation. Even the maneuver continues, the estimation algorithm stops at 8 km before the stationary target. In this way, the divergency due to the unobservability for the maneuver obtained by MPNG and also error in filtering LOS angle for the sinusoidal motion are prevented. Both of the scenario maneuvers are started at 8 km from the initial missile position (0,0).

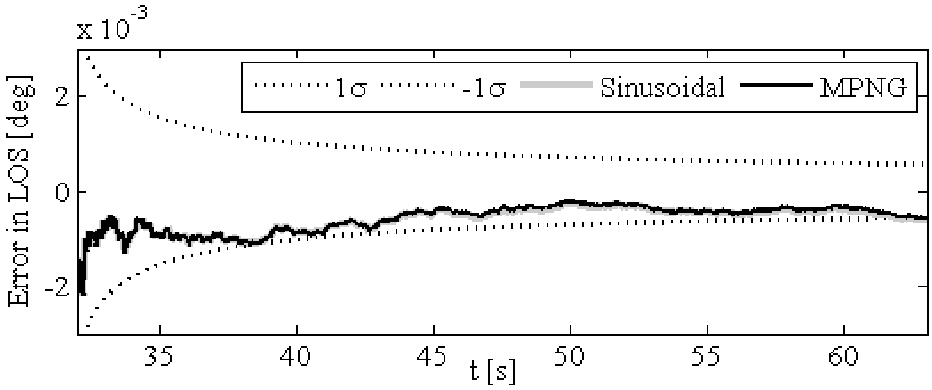

Figure 4.4-2 Error in LOS angle

Figure 4.4-2 shows the error covariance of the LOS angle and there is no filtering difference between the MPNG and the sinusoidal motion since the estimation is stopped before the system becomes unobservable for the MPNG-maneuver and before the linearization error becomes dominant for the sinusoidal motion.

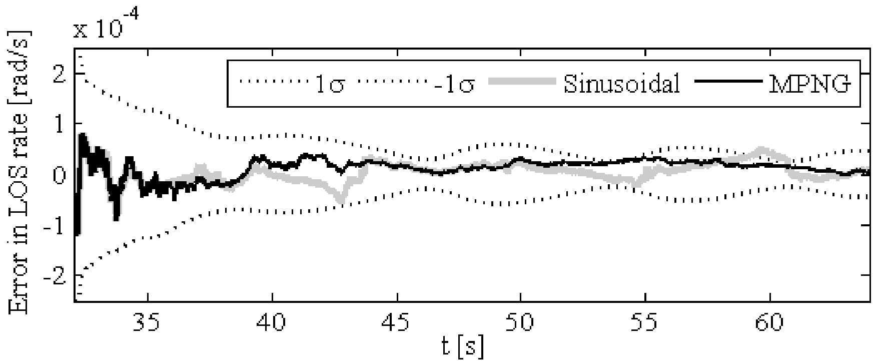

Figure 4.4-3 Error in LOS rate

In Figure 4.4-3, the error covariance of the LOS rate is given. It could be interpreted that there is no difference between the two types of maneuvers when they are filtering the LOS rate measurement.

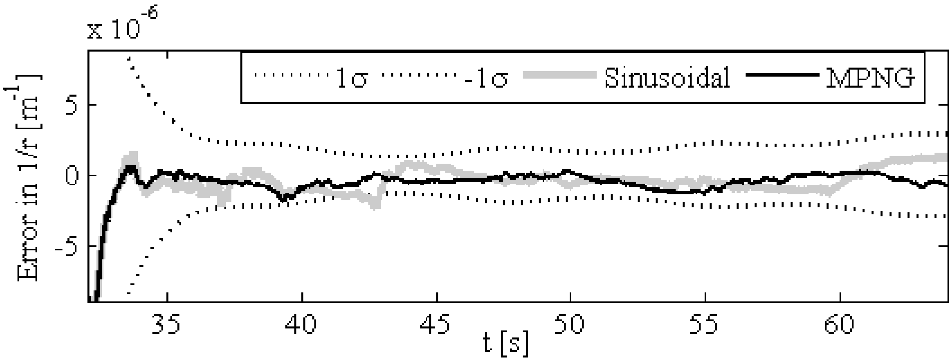

Figure 4.4-4 Error in 1/r

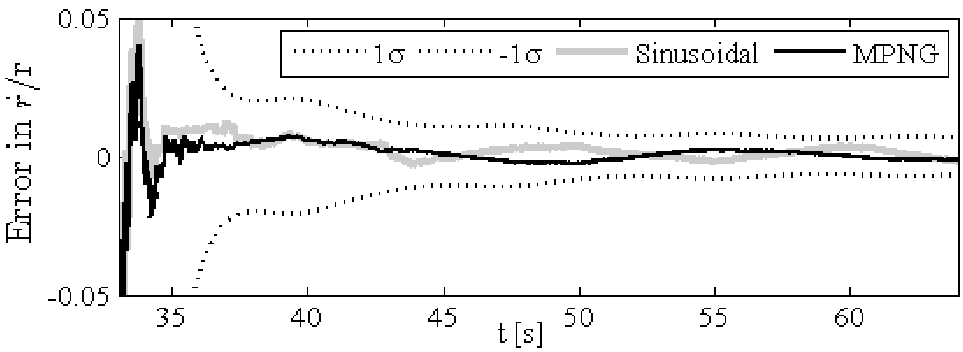

Figure 4.4-5 Error in $\dot{r}/r$

In Figure 4.4-4 the error covariance of 1/r is given. Since the estimation is stopped before the system become unobservable and the small angle assumption is violated, estimation results of the range are almost the same.

Figure 4.4-5 shows the error in $\dot{r}/r$. It is seen that there is no estimation difference between the two maneuvers. Despite the fact that the maneuvers continue through the end of the flight, since the estimation is limited between 8 km from the origin and 8 km before the stationary target, the error covariance results for all states of the estimation problem are the same as expected. After this point on, effects of maneuver types on range estimation are analyzed with Mach number, angle of attack (alpha), side slip angle (beta), Euler angles and acceleration command history.

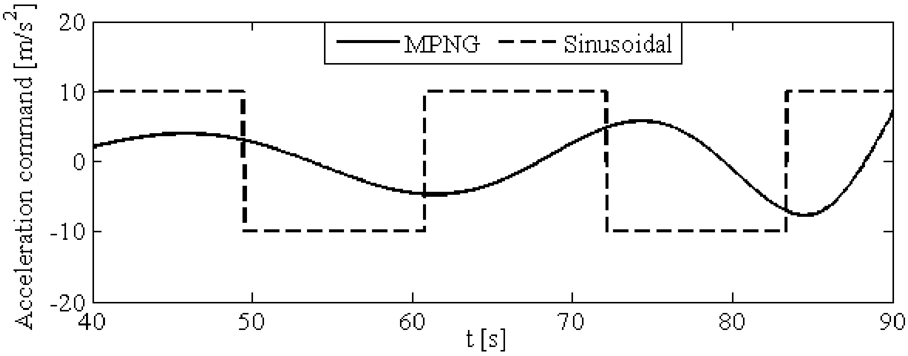

Figure 4.4-6 Acceleration command history for different maneuver types

Figure 4.4-6 demonstrates the acceleration command history which shows that less effort is needed for MPNG. Since the sea skimming anti-ship missile has turbojet, there will be less fuel consumption to get oscillatory motion. In this way the missile can be launched with less fuel.

Flight paths for both maneuvers are given in Figure 4.4-1 before. Maneuver with MPNG has less amplitude than the sinusoidal motion in the east axis due to its oscillatory nature. Decrease in maneuver amplitude results with less side slip angle and the results for the side slip angles are given in Figure 4.4-7. While side slip angle for MPNG varies between [-1.5 +1.5] degree, it is [-3 +3] degree for the sinusoidal motion. This causes less drag force for the missile in MPNG case.

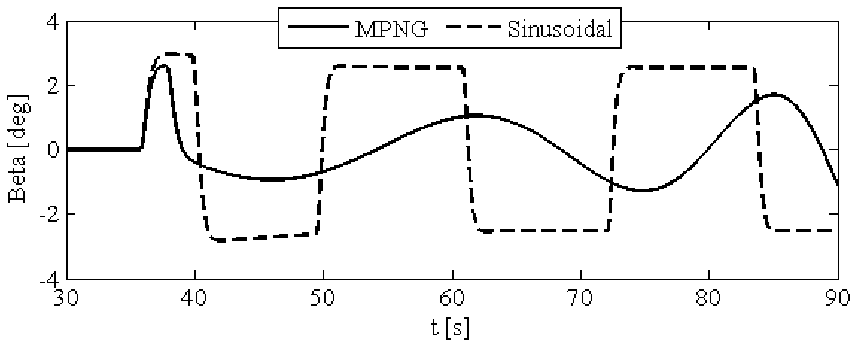

Figure 4.4-7 Beta for two maneuver types

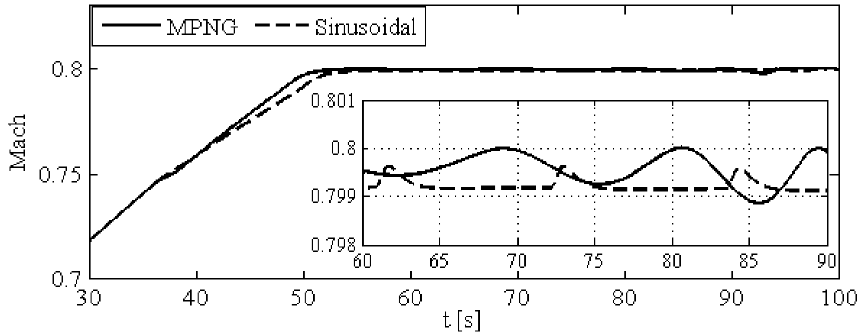

Figure 4.4-8 Mach profile for two maneuver types

Figure 4.4-8 shows the Mach profile for both the MPNG and the sinusoidal motion. From the 30th second to 50th second turbojet engine of the missile tries to increase the velocity to the commanded mach of 0.8 and MPNG allows reaching to the commanded Mach number faster than the maneuver by sinusoidal motion. Moreover, the maneuver obtained by using MPNG results in less undesired descends in Mach number.

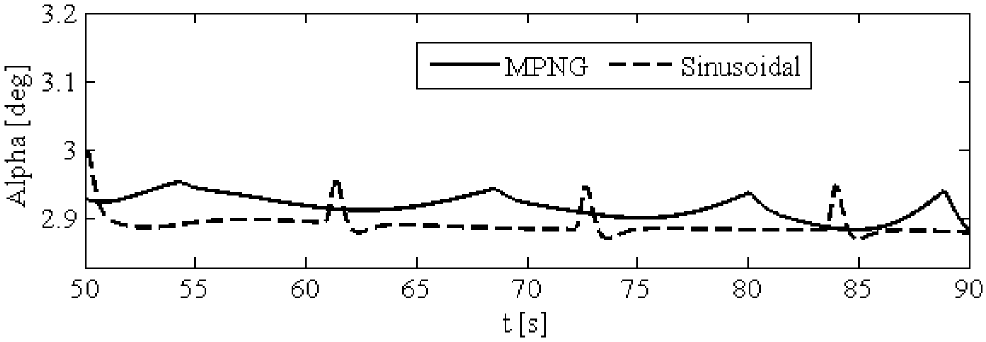

Figure 4.4-9 Alpha for two maneuver types

Figure 4.4-9 shows the alpha profile for two types of maneuver. Since the analyzed missile in this thesis is a sea skimming missile, motion in elevation channel is not included to the estimation filters and so it is not expected to observe different alpha values for two types of maneuver. The alpha vs. time graph supports this argument because alpha profile is almost the same for two maneuver types.

Figure 4.4-10 demonstrates the Euler angles for both maneuvers generated by the MPNG and by the sinusoidal motion. While the missile maneuvers in yaw channel, due to the coupled dynamics of the missile, a small roll angle is induced in the system and it is bigger for the sinusoidal motion than the MPNG case. The missile studied in this thesis maneuvers only in the yaw channel. Moreover, in Figure 4.4-10 part (c), the maneuver obtained by the MPNG causes smaller yaw angle and this results in less drag force.

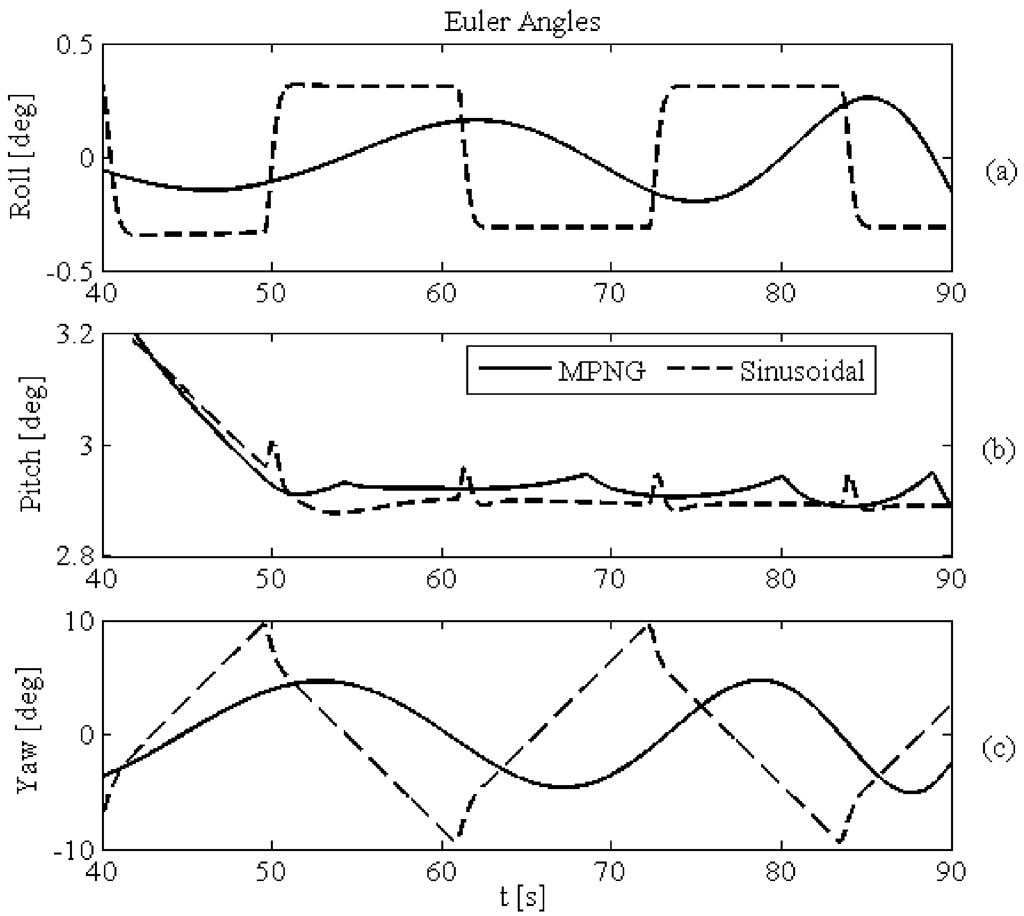

Figure 4.4-10 Euler angles for two maneuver types

CHAPTER 5

CONCLUSION

In this thesis, estimation of the relative range between a target and the missile is studied. The estimation is performed by using the measurements obtained from a RF seeker and missile acceleration information obtained from IMU. The tracking missile is assumed to be a sea skimming anti-ship missile.

The main problem for the angle-only target tracking is the observability. If the tracking filter is not observable then the filter starts to diverge. To ensure the observability through the estimation the missile has to maneuver. Two different maneuver types are studied throughout this thesis; the sinusoidal motion and the oscillatory flight path generation for the missile by using the modified proportional navigation guidance law. The effects of maneuver type on the estimation performance are also investigated within the scope of this thesis.

Two different approaches for range estimation are investigated and compared using simulated data: the standard Extended Kalman Filter (EKF) and the Neural Extended Kalman Filter (NEKF). The NEKF has an adaptive nature and this nature is used to prevent estimation from the errors occurred due to the linearization or the mismodeling of the system. When sinusoidal motion is performed by the missile to enhance the observability, the LOS angle increases through the end of the flight and this situation causes a linearization error for the error covariance update of the estimation. As the LOS angle increases, the system moves off the linearization point and the filtering performance of the measurements decreases which also affects the estimation performance of the other states. In such cases, the NEKF proved that it compensated the unmodelled dynamics of the plant or the linearization error by learning online. Another feature of the NEKF arises when the MPNG is used to execute the missile maneuver. It is mentioned before that the MPNG causes oscillatory motion and when the missile is getting closer to the target, amplitude of the oscillatory motion starts to decrease which results in loss in observability. When the system is unobservable, the NEKF cannot train its weights and hence, the NEKF has rapidly increasing covariance error and the error becomes larger than the error of the EKF. Main reason of this is the coupled states and the weights of the NEKF. Moreover, the error covariance increment cannot be decreased without observability.

Another issue worked in this thesis is the maneuver type of the missile to obtain observability. Sinusoidal motion generated with the open-loop acceleration commands and the closed loop maneuvers of MPNG are investigated. Since the scope of thesis the estimation with NEKF, maneuver type analysis is completed with the NEKF. It is mentioned that the linearization error in covariance update of the filter becomes apparent through the end of the flight for the sinusoidal motion and it brings about observability problem for the oscillatory motion. In order to evaluate both maneuver types equally, the estimation is stopped before linearization and the observability problems are emerged. After setting the same conditions for the analyzed maneuvers, the MPNG shows advantages for the EKF. First, the sinusoidal motion is executed by open-loop acceleration commands but the oscillatory motion has closed-loop nature. This feature is quite important for the target hitting efficiency. Another advantage of the oscillatory motion includes the aerodynamic efficiency. While the amplitude of the maneuver decrease, the missile is exposed to less beta angle which helps to reduce the aerodynamic drag force applied on the missile. Reduction in the aerodynamic drag force results with less fuel consumption which is more desired.

REFERENCES

[1] S. Kale “Hibrit Ölçümlerde Hedef Kestirim Algoritması Tasarımı”, Havacılık ve Uzay Teknolojileri Dergisi, Temmuz 2014, Cilt 7, Sayı 2 (103-110).

[2] Y. Bar- Shalom and X Li, Estimation and Tracking: Principles, Techniques, and Software, Artech House, 1993.

[3] Blackman and R. Popoli, Design and Analysis of Modern Tracking Systems, Artech House, 1999.

[4] B. Ristic, S. Arulampalam, and N. Gordon, Beyond the Kalman Filter, Partical Filters for Tracking Application, Artech House, 2004.

[5] Aidala, V. J., "Kalman Filter Behavior in Bearings-Only Tracking Applications", IEEE Transactions on Aerospace and Electronic Systems, Vol. AES-15, July 1979, pp. 29-39.

[6] Aidala, V. J., and Hammel, S. E., "Utilization of Modified Polar Coordinates for Bearings-Only Tracking", IEEE Transactions on Automatic Control, Vol. AC-28, Aug. 1983, pp. 283-294.

[7] S. C Nardone, V. J.Aidala, "Observability Criteria for Bearings-Only Target Motion Analysis", IEEE Transactions on Aerospace and Electronic Systems, Vol. 17, No. 2, 1981.

[8] Hammel, S. E., and Aidala, V. J.,”Observability Requirements for Three-Dimensional Tracking via Angle Measurements”, IEEE Transactions on Aerospace and Electronic Systems, Vol. 21, No. 2, 1985.

[9] Fogel, E.,Gavish, M.,”Nth-Order Dynamics Target Observability from Angle Measurements”, IEEE Transactions on Aerospace and Electronic Systems, Vol. 24, No. 3, 1988.

[10] Gorecki, F. D., “More on Angle-Only-Track, Observability and Information theory”, AIAA Guidance, Navigation and Control Conference, 1990.

[11] Song, T. L., “Observability of Target Tracking with Bearing-Only Measurements”, IEEE Transactions on Aerospace and Electronic Systems, Vol. 32, No. 4, 1996.

[12] Jauffret, C. and Pillon, D.,”Observability in Passive Target Motion Analysis”, IEEE Transactions on Aerospace and Electronic Systems, Vol. 32, No. 4, 1996.

[13] Aidala, V. J., "Kalman Filter Behavior in Bearings-Only Tracking Applications", IEEE Transactions on Aerospace and Electronic Systems, Vol. AES-15, July 1979, pp. 29-39.

[14] M. Thank, H. Ryu, E. Song. “Observability Characteristics of Angle-Only Measurement under Proportional Navigation”, 34st Society of Instrument and Control Engineers Conference, 1995.

[15] Taur, D. and Chern J., “Passive Ranging For Dog-Fight Air-to-Air IR Missiles”, AIAA Guidance, Navigation and Control Conference, 1999.

[16] Song, T. L. “Target Adaptive Guidance for Passive Homing Missiles”, IEEE Transactions on Aerospace and Electronic Systems, Vol. AES-33, January 1997, pp. 312-316.

[17] Song, T. L. “Practical Guidance for Homing Missiles With Bearing-Only Measurements”, IEEE Transactions on Aerospace and Electronic Systems, Vol. AES-32, January 1996, pp. 434-443.

[18] Wabgaonkar, H. and Stubberud, A. “Approximation and Estimation Techniques for Neural Networks”, IEEE Transactions on Aerospace and Electronic Systems, December 1990, pp. 2736-2740.

[19] Stubberud, S. C., Lobbia, R. N. and Owen, M. “An Adaptive Extended Kalman Filter Using Artificial Neural Networks”, IEEE Transactions on Aerospace and Electronic Systems, Vol. 2, December 1995, pp. 1852-1856.

[20] Singhal, S. and Wu, L. “Training Multilayer Perceptron with the Extended Kalman Algorithm”, Advance in Neural Information Processing systems 1, 1989, pp. 133-140.

[21] Stubbered, S. C., Kramer, K. A. and Geremia, J. A., ”On-line Sensor Modeling Using a Neural Kalman filter”, IEEE Instrumentation and Measurement Technology Conference, 2006, pp. 969-974.

[22] Stubbered, S. C., Kramer, K. A. and Geremia, J. A., ”Target Registration Correction using the neural Extended Kalman filter”, IEEE Computational Intelligence for Measurement Systems and Applications, 2006, pp. 51-56.

[23] Wong, Y. C. and Sundareshan, M. K., “Data fusion and tracking of Complex target Maneuvers with a Simplex-Trained Neural Network-Based Architecture", IEEE Neural Networks Proceedings, 1988, pp. 1024-1029.

[24] Stubbered, S. C. and Owen, M. W., “Targeted On-line Modeling for an Extended Kalman Filter using Artificial Neural Networks”, IEEE Neural Networks Proceedings, 1988, pp. 1019-1023.

[25] Stubbered, S. C. and Owen, M. W., “A Neural Extended Kalman Filter Multiple Model Tracker”, IEEE Vol. 4, 2003, pp. 2111-2119.

[26] Stubbered, S. C., Kramer, K. A. “Tracking of Multiple Target Types with a Single Neural Extended Kalman Filter”, IEEE Intelligent Systems, 2006, pp. 463-468.

[27] Stubbered, S. C. and Owen, M. W., “Interacting Multiple Model Tracking using a neural Extended Kalman Filter”, IEEE Neural Networks, 1999, pp. 2788-2791.

[28] Stubbered, S. C., Kramer, K. A. “A 2-D Intercept Problem Using the Neural Extended Kalman Filter for Tracking and Linear Predictions”, IEEE 2005.

[29] Stubbered, S. C., Kramer, K. A. “Impact Time and Point Predicted Using a Neural Extended Kalman Filter”, IEEE Intelligent Sensors, Sensor Networks and Information Processing Conference, 2005, pp. 199-204.

[30] Güvenç, S. K. “Range-to-go Estimation for a Tactical Missile with a Passive Seeker”, Master Thesis, METU, 2015.

[31] Peach, N. “Bearing-Only tracking Using a Set of Range-Parameterised Extended Kalman Filters”, IEEE Control Theory and Applications, Vol. 142, January 1995, pp. 73-80.

[32] Ross, R. A. and Samuel, S. B. “Implementation of an Angle-Only Tracking filter”, Signal and Data Processing of Small Targets, Vol. 1481, April 01, 1991.

[33] Taur, D. and Chern, J., “Practical Passive Ranging with Bearing-Only Measurement for IRST”, AIAA Guidance, Navigation and Control Conference, 14-17 August 2000.

[34] Erlandsson, T., “Angle-Only Target Tracking”, Master Thesis, Linköpings University Department of Electrical Engineering, 2007, Thesis Number: LITH-ISY-EX-07/3904-SE.

APPENDIX A

DERIVATIONS

A.1 Derivation of State Equations in MSC

This part of the appendix shows the derivation of state equation for angle-only target tracking in MSC.

$\dot{y}_4$ which is $\ddot{\lambda}$. is derived as

$$\frac{d}{dt}(y_4) = \frac{d}{dt}(\dot{\lambda}) = \frac{d}{dt}\left[\frac{d}{dt}\arctan\left(\frac{r_x}{r_y}\right)\right] = \frac{d}{dt}\left[\frac{1}{1+\left(\frac{r_x}{r_y}\right)^2}\cdot\frac{\dot{r}_x r_y - \dot{r}_y r_x}{r_y^{\,2}}\right] = \frac{d}{dt}\left[\frac{\dot{r}_x r_y - \dot{r}_y r_x}{r_x^{\,2} + r_y^{\,2}}\right] \quad \text{(A.1)}$$

$$\frac{d}{dt}(y_4) = \frac{\left(r_x^{\,2} + r_y^{\,2}\right)\frac{d}{dt}\left[\dot{r}_x r_y - \dot{r}_y r_x\right] - \left(\dot{r}_x r_y - \dot{r}_y r_x\right)\frac{d}{dt}\left[r_x^{\,2} + r_y^{\,2}\right]}{\left(r_x^{\,2} + r_y^{\,2}\right)^2} \quad \text{(A.2)}$$

$$\frac{d}{dt}(y_4) = \frac{\left(\ddot{r}_x r_y + \dot{r}_x \dot{r}_y - \dot{r}_x \dot{r}_y - r_x \ddot{r}_y\right)\left(r_x^{\,2} + r_y^{\,2}\right) - 2\left(r_y \dot{r}_y + r_x \dot{r}_x\right)\left(\dot{r}_x r_y - \dot{r}_y r_x\right)}{\left(r_x^{\,2} + r_y^{\,2}\right)^2} \quad \text{(A.3)}$$

$$\frac{d}{dt}(y_4) = \frac{\left(\ddot{r}_x r_y - r_x \ddot{r}_y\right)}{\left(r_x^{\,2} + r_y^{\,2}\right)} - 2\frac{\left(r_y \dot{r}_y + r_x \dot{r}_x\right)\left(\dot{r}_x r_y - \dot{r}_y r_x\right)}{\left(r_x^{\,2} + r_y^{\,2}\right)^2} \quad \text{(A.4)}$$

and also

$$r = \sqrt{r_x^{\,2} + r_y^{\,2}}$$
$$r_x = r\sin(\lambda) \qquad (A.5)$$
$$r_y = r\cos(\lambda)$$

$$a_x = \ddot{r}_x$$
$$a_y = \ddot{r}_y \qquad (A.6)$$

$$\dot{\lambda} = \frac{\left(\dot{r}_x r_y - \dot{r}_y r_x\right)}{\left(r_x^{\,2} + r_y^{\,2}\right)} \qquad (A.7)$$

After inserting above relations into $\frac{d}{dt}\left(y_4\right)$ then it is obtained that

$$\frac{d}{dt}\left(y_4\right) = \frac{r\left(a_x\cos(\lambda) - a_y\sin(\lambda)\right)}{r^2} - 2\frac{\left(r_x\dot{r}_x + r_y\dot{r}_y\right)\dot{\lambda}}{r^2} \qquad (A.8)$$

$$\frac{d}{dt}\left(y_4\right) = y_1\left[a_x\cos(\mathrm{y}_2) - a_y\sin(\mathrm{y}_2)\right] - 2\frac{\left(r_x\dot{r}_x + r_y\dot{r}_y\right)y_4}{r^2} \qquad (A.9)$$

To get more simple form, y_3 is written as

$$y_3 = \frac{\dot{r}}{r} = \frac{1}{\sqrt{r_x^{\,2} + r_y^{\,2}}}\frac{d}{dt}\left(\sqrt{r_x^{\,2} + r_y^{\,2}}\right) = \frac{\left(r_x\dot{r}_x + r_y\dot{r}_y\right)}{r^2} \qquad (A.10)$$

By inserting y_3 into the $\dot{y}_4$, then

$$\dot{y}_4 = -2y_4y_3 + y_1\left[a_x\cos(\mathrm{y}_2) - a_y\sin(\mathrm{y}_2)\right] \qquad (A.11)$$

Continue with the derivation of $\dot{y}_3$

$$\frac{d}{dt}\left(y_3\right) = \frac{d}{dt}\left(\frac{\dot{r}}{r}\right) = \frac{d}{dt}\left(\frac{\left(r_x\dot{r}_x + r_y\dot{r}_y\right)}{r_x^{\,2} + r_y^{\,2}}\right) \qquad (A.12)$$

$$\frac{d}{dt}(y_3)=\frac{\left(r_x^{\,2}+r_y^{\,2}\right)\left(\frac{d}{dt}\left(r_x\dot{r}_x+r_y\dot{r}_y\right)\right)-\left(r_x\dot{r}_x+r_y\dot{r}_y\right)\left(\frac{d}{dt}\left(r_x^{\,2}+r_y^{\,2}\right)\right)}{\left(r_x^{\,2}+r_y^{\,2}\right)^2} \tag{A.13}$$

$$\frac{d}{dt}(y_3)=\frac{\left(\dot{r}_x^{\,2}+r_x\ddot{r}_x+\dot{r}_y^{\,2}+r_y\ddot{r}_y\right)\left(r_x^{\,2}+r_y^{\,2}\right)-2\left(r_x\dot{r}_x+r_y\dot{r}_y\right)\left(r_x\dot{r}_x+r_y\dot{r}_y\right)}{\left(r_x^{\,2}+r_y^{\,2}\right)^2} \tag{A.14}$$

$$\frac{d}{dt}(y_3)=\frac{\left(\dot{r}_x^{\,2}+\dot{r}_y^{\,2}\right)\left(r_x^{\,2}+r_y^{\,2}\right)}{\left(r_x^{\,2}+r_y^{\,2}\right)^2}+\frac{\left(r_x\ddot{r}_x+r_y\ddot{r}_y\right)\left(r_x^{\,2}+r_y^{\,2}\right)}{\left(r_x^{\,2}+r_y^{\,2}\right)^2}-2\frac{\left(r_x\dot{r}_x+r_y\dot{r}_y\right)^2}{\left(r_x^{\,2}+r_y^{\,2}\right)^2} \tag{A.15}$$

$$\frac{d}{dt}(y_3)=\frac{\left(\frac{d}{dt}\left(r\sin(\mathrm{y}_2)\right)\right)^2}{r_x^{\,2}+r_y^{\,2}}+\frac{a_x\sin(\mathrm{y}_2)+a_y\cos(\mathrm{y}_2)}{r}-2\frac{\dot{r}^2}{r^2} \tag{A.16}$$

$$\frac{d}{dt}(y_3)=\frac{\dot{r}^2+r^2\dot{y}_2}{r^2}+\frac{a_x\sin(\mathrm{y}_2)+a_y\cos(\mathrm{y}_2)}{r}-2\frac{\dot{r}^2}{r^2} \tag{A.17}$$

At the end of these procedures it is obtained that

$$\dot{y}_3=y_4^{\,2}-y_3^{\,2}+y_1\left[a_x\sin(\mathrm{y}_2)+a_y\cos(\mathrm{y}_2)\right] \tag{A.18}$$

For the derivative of first state $\dot{y}_1$

$$\dot{y}_1=\frac{d}{dt}\left(\frac{1}{r}\right)=\frac{-\dot{r}}{r^2}=-\left(\frac{\dot{r}}{r}\right)\left(\frac{1}{r}\right)=-y_3y_1 \tag{A.19}$$

Finally continuous time state equation used in this thesis for 2D target tracking problem is

$$\begin{aligned}
\dot{y}_1 &= -y_3y_1\\
\dot{y}_2 &= y_4\\
\dot{y}_3 &= y_4^{\,2}-y_3^{\,2}+y_1\left[a_x\sin\left(y_2\right)+a_y\cos\left(y_2\right)\right]\\
\dot{y}_4 &= -2y_4y_3+y_1\left[a_x\cos\left(y_2\right)-a_y\sin\left(y_2\right)\right]
\end{aligned} \tag{A.20}$$

A.2 Derivation of Jacobian J_f and J_c

From equation (A.20) continuous time J_f can be calculated as

$$J_f\left(y_1,y_2,y_3,y_4\right)=\begin{pmatrix} \frac{\partial \dot{y}_1}{\partial y_1} & \cdots & \frac{\partial \dot{y}_1}{\partial y_4} \\ \vdots & \ddots & \vdots \\ \frac{\partial \dot{y}_4}{\partial y_1} & \cdots & \frac{\partial \dot{y}_4}{\partial y_4} \end{pmatrix}=\begin{pmatrix} J_{f11} & J_{f12} & J_{f13} & J_{f14} \\ J_{f21} & J_{f22} & J_{f23} & J_{f23} \\ J_{f31} & J_{f32} & J_{f33} & J_{f34} \\ J_{f41} & J_{f42} & J_{f43} & J_{f44} \end{pmatrix} \quad (A.21)$$

$$J_f\left(y_1,y_2,y_3,y_4\right)=\begin{pmatrix} -y_3 & 0 & -y_1 & 0 \\ 0 & 0 & 0 & 1 \\ a_x y_2+a_y & y_1\left(a_x-y_2a_y\right) & -2y_3 & 2y_4 \\ a_x-a_y y_2 & y_1\left(-a_x y_2-a_y\right) & -2y_4 & -2y_3 \end{pmatrix} \quad (A.22)$$

(A.22) is in the form of continuous-time. It should be discretized to use it in Matlab environment. Also, J_c is the Jacobian of measurement equation.

A.3 Representation of Process Noise Q in MSC

Process noise Q is defined in Cartesian coordinates in this thesis and it should be represented in MSC. Transformation from polar coordinates to Cartesian coordinates can be written as

$$y=\begin{bmatrix} y_1 \\ y_2 \\ y_3 \\ y_4 \end{bmatrix}=\begin{bmatrix} \frac{1}{r} \\ \lambda \\ \frac{\dot{r}}{r} \\ \dot{\lambda} \end{bmatrix}=\begin{bmatrix} \left(x_1^2+x_2^2\right)^{-1/2} \\ \arctan\left(\frac{x_1}{x_2}\right) \\ \frac{x_1x_3+x_2x_4}{x_1^2+x_2^2} \\ \frac{x_3x_2-x_4x_1}{x_1^2+x_2^2} \end{bmatrix} \quad (A.23)$$

To transform Q_{car} to Q_{msc}

$$Q_{msc} = J_y Q_{car} J_y^T \tag{A.24}$$

where J_y is given below.

$$J_y\left(x_1, \mathrm{x}_2, \mathrm{x}_3, \mathrm{x}_4\right) = \begin{pmatrix} \frac{\partial y_1}{\partial x_1} & \cdots & \frac{\partial y_1}{\partial x_4} \\ \vdots & \ddots & \vdots \\ \frac{\partial y_4}{\partial x_1} & \cdots & \frac{\partial y_4}{\partial x_4} \end{pmatrix} = \begin{pmatrix} J_{y11} & J_{y12} & J_{y13} & J_{y14} \\ J_{y21} & J_{y22} & J_{y23} & J_{y23} \\ J_{y31} & J_{y32} & J_{y33} & J_{y34} \\ J_{y41} & J_{y42} & J_{y43} & J_{y44} \end{pmatrix} \tag{A.25}$$

$$\begin{aligned} J_{y11} &= -\frac{x_1}{\left(x_1^{\ 2} + x_2^{\ 2}\right)^{3/2}} \\ J_{y12} &= -\frac{x_2}{\left(x_1^{\ 2} + x_2^{\ 2}\right)^{3/2}} \\ J_{y13} &= J_{y14} = 0 \end{aligned} \tag{A.26}$$

$$\begin{aligned} J_{y21} &= \frac{1}{x_2\left(\frac{x_1^{\ 2}}{x_2^{\ 2}} + 1\right)} \\ J_{y22} &= -\frac{x_1}{\left(x_1^{\ 2} + x_2^{\ 2}\right)} \\ J_{y23} &= J_{y24} = 0 \end{aligned} \tag{A.27}$$

$$\begin{aligned} J_{y31} &= \frac{x_3}{\left(x_1^{\ 2} + x_2^{\ 2}\right)} - \frac{2x_1\left(x_1x_3 + x_2x_4\right)}{\left(x_1^{\ 2} + x_2^{\ 2}\right)^2} \\ J_{y32} &= \frac{x_4}{\left(x_1^{\ 2} + x_2^{\ 2}\right)} - \frac{2x_2\left(x_1x_3 + x_2x_4\right)}{\left(x_1^{\ 2} + x_2^{\ 2}\right)^2} \\ J_{y33} &= \frac{x_1}{\left(x_1^{\ 2} + x_2^{\ 2}\right)} \\ J_{y34} &= \frac{x_2}{\left(x_1^{\ 2} + x_2^{\ 2}\right)} \end{aligned} \tag{A.28}$$

$$
\begin{aligned}
J_{y41} &= \frac{2x_1\left(x_1x_4 - x_2x_3\right)}{\left(x_1^{\ 2} + x_2^{\ 2}\right)^2} - \frac{x_4}{\left(x_1^{\ 2} + x_2^{\ 2}\right)} \\
J_{y42} &= \frac{2x_2\left(x_1x_4 - x_2x_3\right)}{\left(x_1^{\ 2} + x_2^{\ 2}\right)^2} + \frac{x_3}{\left(x_1^{\ 2} + x_2^{\ 2}\right)} \\
J_{y43} &= \frac{x_2}{\left(x_1^{\ 2} + x_2^{\ 2}\right)} \\
J_{y44} &= -\frac{x_1}{\left(x_1^{\ 2} + x_2^{\ 2}\right)}
\end{aligned}
\qquad \text{(A.29)}
$$